12-2012

Techniques for Wireless Channel Modeling in Harsh Environments

Phani Teja Kuruganti
pkurugan@utk.edu

To the Graduate Council:

I am submitting herewith a dissertation written by Phani Teja Kuruganti entitled "Techniques for Wireless Channel Modeling in Harsh Environments." I have examined the final electronic copy of this dissertation for form and content and recommend that it be accepted in partial fulfillment of the requirements for the degree of Doctor of Philosophy, with a major in Electrical Engineering.

Seddik Djouadi, Major Professor

We have read this dissertation and recommend its acceptance:

Aly Fathy, Rapinder Sawhney, Husheng Li, James Nutaro

Accepted for the Council:

Carolyn R. Hodges

Vice Provost and Dean of the Graduate School

(Original signatures are on file with official student records.)

Techniques for Wireless Channel Modeling in Harsh Environments

A Dissertation

Presented for the

Doctor of Philosophy

Degree

The University of Tennessee, Knoxville

Phani Teja Kuruganti

December 2012

To my mother and father

Swarajya Lakshmi and Late Prabhakar Sastry

Acknowledgements

Foremost, I would like to express my deepest gratitude to my advisor, Dr. Seddik Djouadi, for his excellent guidance, endless support, and thought provoking discussions during my graduate study and research at the University of Tennessee, Knoxville. His sharp sense of humor and camaraderie has gone a long way in making my graduate study an enjoyable and memorable experience. I also wish to thank Dr. Jim Nutaro for his support and guidance through the research. My deepest gratitude for all the valuable discussions and truly supported me as a sounding board for ideas for research. I also wish to give my thanks to Dr. Aly Fathy, Dr. Husheng Li, Dr. Rupy Sawhney for serving on my dissertation committee.

I'm deeply indebted to my parents, Swarajya Lakshmi and Prabhakar Sastry, for the support and the encouragement they provided to me to explore higher levels of education. My special thanks to my wonderful sisters, Srilalitha and Srivalli, who always give me their unconditional support through my life. I would like to deeply appreciate all my friends in Knoxville who are like family and certainly made my journey through school a pleasurable experience.

I would like to thank my true mentors Glenn Allgood and Wayne Manges for their extraordinary support and always encouraging me to pursue PhD. I would like to thank Oak Ridge National Laboratory for support during these studies. I would like to express my deepest regards to David Hetrick for supporting my education and I have learned a lot from his leadership at Oak Ridge National Laboratory.

Finally, I would like to express my deepest gratitude and love to my wife, Kusum, for her support and understanding. I will spend the rest of my life showing my appreciation.

I learned very early the difference between knowing the name of something and knowing something.

- Richard Feynman

Abstract

With the rapid growth in the networked environments for different industrial, scientific and defense applications, there is a vital need to assure the user or application a certain level of Quality of Service (QoS). Environments like the industrial environment are particularly harsh with interference from metal structures (as found in the manufacturing sector), interference generated during wireless propagation, and multipath fading of the radio frequency (RF) signal all invite novel mitigation techniques. The challenge of achieving the benefits like improved energy efficiency using wireless is closely coupled with maintaining network QoS requirements. Assessment and management of QoS needs to occur, allowing the network to adapt to changes in the RF, information, and operational environments. The capacity to adapt is paramount to maintaining the required operational performance (throughput, latency, reliability and security).

This thesis address the need for accurate radio channel modeling techniques to improve the performance of the wireless communication systems. Multiple different channel modeling techniques are considered including statistical models, ray tracing techniques, finite time-difference technique, transmission line matrix method (TLM), and stochastic differential equation-based (SDE) dynamic channel models. Measurement of ambient RF is performed at several harsh industrial environments to demonstrate the existence of uncertainty in channel behavior. Comparison of various techniques is performed with metrics including accuracy, applicability, and computational efficiency. SDE- and TLM-based methods are validated using indoor

and outdoor measurements. Fast, accurate techniques for modeling multipath fading in harsh environments is explored. Application of dynamic channel models is explored for improving QoS of wireless communication system.

The TLM-based models provide accurate site-specific path loss calculations taking into consideration materials and propagation characteristics of propagating environment. The validation studies confirm the technique is comparable with existing channel models. The TLM-based channel models is extended to compute the site-specific multipath characteristics of the radio channel eliminating the need for experimental measurement. The TLM-based simulator is also integrated with packet-level network simulator to perform end to end-to-end site specific calculation of wireless network performance. The SDE-channel models provide accurate online estimations of the channel performance along with accurate one-step prediction of the signal strength. The validation studies confirm the accuracy of the technique. Application of the SDE-based models for adaptive antenna control is formulated using online recursive estimation.

Contents

List of Tables

List of Figures

Chapter 1

Introduction

Wireless technology is fueling new paradigms in government, personal, commercial, and industrial communication systems throughout the marketplace. The industrial community is poised to adopt wireless technology to support technical innovations, e.g., widespread use of wireless sensors forecasted to improve manufacturing production and energy efficiency and reduce emissions[39]. Mobile broadband networks have revolutionized information access and personal communications, virtually changing the culture. Wireless sensors provide better process visibility (*in situ* sensing) to facilitate better control systems and inferential process control systems. The result will be improved process and energy efficiencies and reduced emissions.

With the rapid growth in the networked environments for different industrial, scientific and defense applications, there is a vital need to assure the user or application a certain level of Quality of Service (QoS). Environments like the industrial environment are particularly harsh with interference from metal structures etc. (as found in the manufacturing sector), interference generated during wireless propagation, and multipath fading of the radio frequency (RF) signal all invite novel mitigation techniques. The challenge of achieving benefits like improved energy efficiency using wireless is closely coupled with maintaining network QoS requirements. Assessment and management of QoS needs to occur, allowing the

network to adapt to changes in the RF, information, and operational environments. The capacity to adapt is paramount to maintaining the required operational performance (throughput, latency, reliability and security).

Wireless communication channels encompass the link between transmitter and receiver antennas. Understanding the electromagnetic wave propagation and information-theoretic capacities of wireless channels is necessary for successfully deploying wireless networks for the above-mentioned applications. The performance of a channel is influenced by the physics of the environment, interference sources, and coexistence of different wireless networks. Often times the channel has varying characteristics over time due to changing interferers and physical changes in the environment. Users of the wireless channel can have limited influence on the performance of the channel. However, accurate representation and understanding of the wireless channel will inevitably help improving the performance of the wireless devices.

1.1 Propagation Modeling Techniques

Propagation of an electromagnetic wave is primarily attributed to three different kinds of phenomena - reflection, diffraction, and scattering[43]. Propagation models have focused on predicting average signal strength at the receiver for a given transmitter distance along with the variation in signal strength as a function of time. Estimating signal strength at a large distance from the transmitter useful in estimating radio coverage is called *large-scale* propagation modeling. Estimating signal variations due to short travel distances over short periods of time is called *small-scale* propagation modeling. Depending on how rapidly the propagating signal changes due to variation in the channel, a channel may be classified as *fast fading* or *slow fading*. The four fundamental parameters used to describe the fading channel are *delay spread, coherence bandwidth, Doppler spread*, and *coherence time*.

Delay spread characterizes the time-dispersive properties of the channel by defining the multipath density in the environment. It is simply the difference between

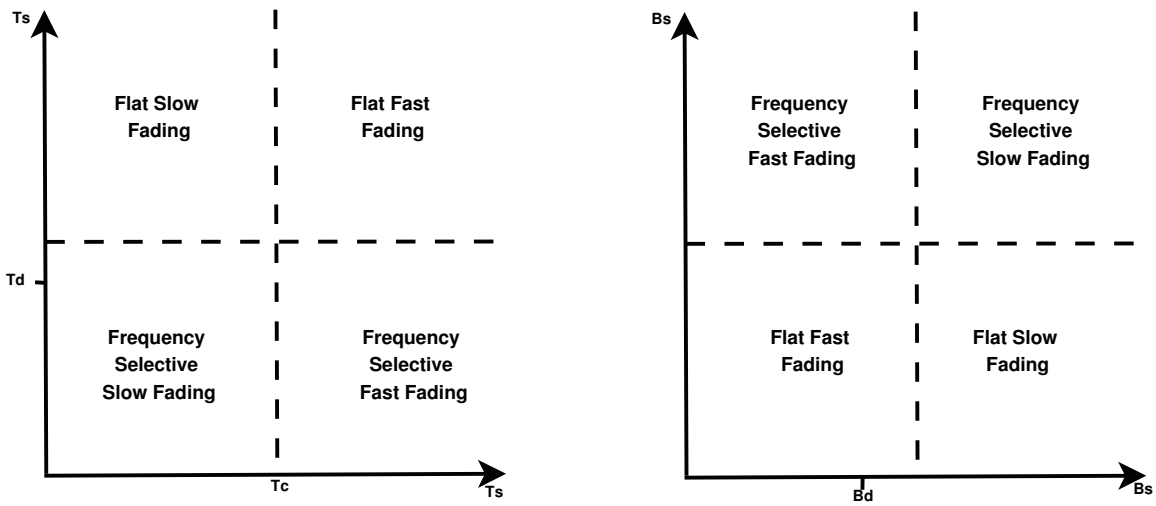

Figure 1.1: Types of Fading Classification

the time of arrival of the first significant multipath component and the time of arrival of the latest multipath component. This is usually obtained by observing the power delay profile (PDP) in channel sounding experiments. Three main parameters observed from the PDP are *mean excess delay, rms delay spread,* and *excess delay spread (X dB)*[43]. Mean excess delay is the first moment of the PDP and defined by

$$\bar{\tau} = \frac{\sum_k P(\tau_k)\tau_k}{\sum_k P(\tau_k)} \tag{1.1}$$

The rms delay spread is the square root of the second central moment of the PDP and is defined by

$$\sigma_\tau = \sqrt{\bar{\tau}^2 - (\bar{\tau})^2} \tag{1.2}$$

Where, $\bar{\tau}$ is the mean excess delay. The maximum excess delay (X dB) of the PDP is the time delay during which the multipath energy falls to X dB below the maximum. The values of the three parameters depend on the choice of noise threshold used to process $P(\tau)$. This threshold is used to differentiate between various received multipath components and thermal noise. If the noise threshold is too low, the noise may be processed as multipath, and the three parameters can be artificially high. The noise threshold is typically related to the receiver sensitivity of the communication

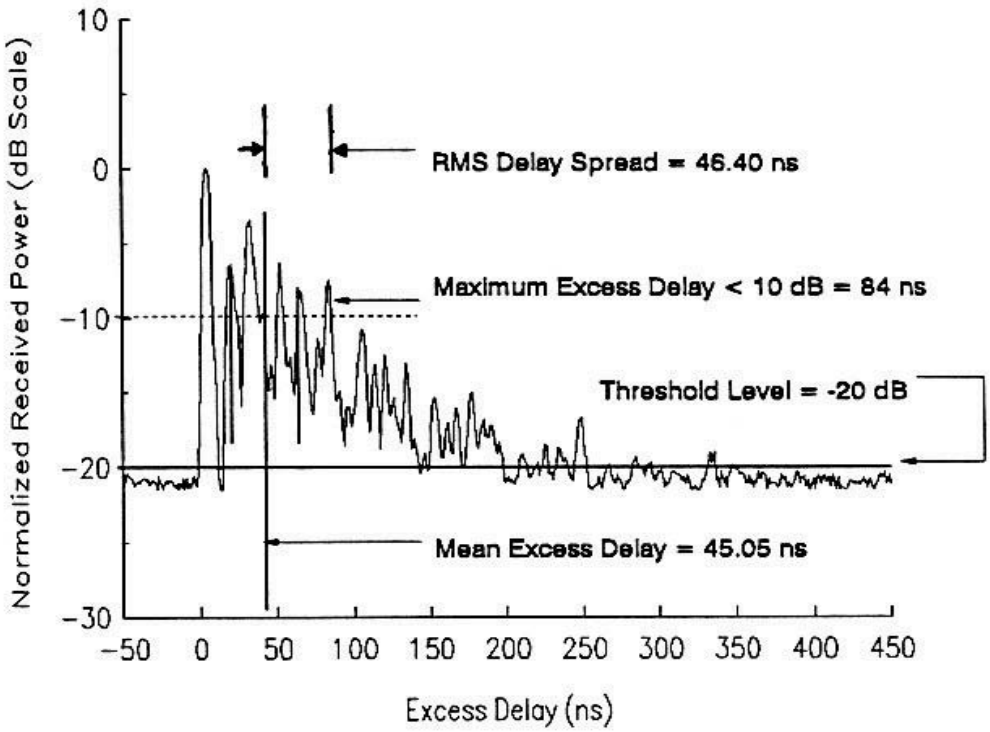

Figure 1.2: Indoor Multipath Measurements

device. Typical receiver sensitivities in IEEE 802.15.4 and IEEE 802.11 devices is -95 dBm. Figure 1.2 shows various multipath metrics for an indoor received signal [43]

Coherence bandwidth is derived from rms delay spread and indicates a statistical measure of the range of frequencies over which the channel is considered to have equal gain and linear phase for all components. Coherence bandwidth is inversely proportional to the delay spread in the channel. A 50% coherence bandwidth is given by

$$B_c = \frac{1}{5\sigma_\tau} \tag{1.3}$$

If the transmitted signal's bandwidth is greater than the 50% coherence bandwidth then the transmitted signal will experience frequency selective fading. If the transmitted signal bandwidth is less than the 50% bandwidth then the transmitted signal will experience flat fading [43].

Doppler spread, B_D, describes the time varying nature of the channel, particularly due to mobility of the receiver or transmitter, and expressed as a range of frequencies over which the received Doppler spectrum is non-zero. When a sinusoidal tone of frequency f_c is transmitted, the Doppler spectrum will have components from $f_c - f_d$ to $f_c + f_d$, where f_d is referred to as Doppler shift. if the baseband signal bandwidth is greater than the Doppler spectrum the effect of the Doppler spread are negligible [43].

Coherence time,T_c, is the measure of the time duration over which the channel impulse response is essentially invariant. The coherence time thereby quantifies the similarity of the channel response at different times. Coherence time is inversely proportional to the maximum doppler shift, f_m experienced by the channel. If the reciprocal of the baseband signal bandwidth is greater than the coherence time of the channel then the signal will experience distortion at the receiver [43].

$$T_C = \frac{1}{f_m} \tag{1.4}$$

While the above four parameters describe the distortion a signal suffers during propagation, the ambient noise plays a significant role in the QoS of a communication system. These noise sources vary from non-communication RF source to multi-band communication systems.

Apart from the characteristics of the channel, there is a significant impact on the communication system when the desired signal is corrupted by another signal at the receiver [26],[29]. Two potential forms of interference sources include (1) wireless networks operating in the same frequency band whose operations are not coordinated, (2) industrial equipment producing wide-band interference in the same frequency band as the communication system.

Federal Communications Commission (FCC) has shared several unlicensed spectrum that can be used for industrial, scientific, and medical (ISM) applications. While ISM bands exist across the FCC spectrum the most commonly used bands

Frequency Range	Center Frequency	Bandwidth
433.050 - 434.790 MHz	433.920 MHz	1.74 MHz
902.000 - 928.000 MHz	915.000 MHz	26 MHz
2.4000 - 2.4835 GHz	2.445 GHz	83.5 MHz
5.725 - 5.875 GHz	5.800 GHz	150 MHz

Table 1.1: Unlicensed ISM Band Frequencies and Bandwidths

are given in Table 1.1. Choice of the frequency of operation impacts the attenuation characteristics of the signal and subsequently the *range* of wireless transmission. Figure 1.7 and Figure 1.8 demonstrate the attenuation of the signal experienced in indoor propagation at 900MHz and 2.45GHz respectively.

Figure 1.3 is a two minute snapshot of the time and frequency domain measurement at the industrial floor of a plastics manufacturing plant. The top portion of the figure indicates the instantaneous time-series signature of the RF channel. The center portion of the signal is a time-frequency spectrogram of the RF channel over two minutes. The bottom part of the figure indicates the frequency domain activity of the RF channel. This measurement is done as part of a survey prior to a IEEE 802.15.4 network installation. The thermal noise floor is at -80dBm while a frequency hopping network used for mobile worker handheld devices occupy the band with peak power at -50dBm. This is a demonstration of the first form of interference as described above. Without better coordination, networks in the same band will incur significant information losses due to collisions.

Significant interference sources exist particularly in the industrial environments that negatively effects the signal-to-noise ratio (SNR) and signal-to-interference ratio (SIR) of the communications systems. Microwave ovens operate in the 2.4GHz band and poor shielding often results in these devices acting as broadband electromagnetic interferers [30]. Figure 1.4 shows the noise patterns generated in the 2.4GHz band by a jet turbine engine. Figure 1.5 shows the periodic burst ultra wide-band noise generated in a coal power plant that shifts the noise floor to -45dBm (from -80dBm). Figure 1.6 demonstrated a periodic wide-band noise generated by an electric arc

furnace in a steel mini mill. Such non-traditional noise sources require careful communication system deployment plan including (1) adaptive frequency/channel hopping to avoid noise band, (2) adaptive time synchronized transmission protocols for transmitting around noise, and (3) advanced spread spectrum modulation techniques with high signal to interference noise ratio (SINR, also called process gain) to accommodate harsh environments.

1.2 Contributions Summary

The contributions of the research undertaken here are as follows:

- RF measurements of various industrial and building environments to understand characteristics of various noise sources and path loss experienced by RF signals in these environments.
- Survey of various channel modeling techniques and comparison of computational needs and accuracy.
- Measurement based validation of the transmission-line matrix method for indoor and outdoor propagation environment.
- Measurement based validation of dynamic channel models using stochastic differential equations for indoor and outdoor propagation environments.
- Fast, accurate method for delay spread estimation for highly reflective environments using transmission-line matrix model.
- End-to-end network simulation of wireless networks using TLM-based propagation models.
- Application of the dynamic channel models towards adaptive array antennas for optimal signal to noise ratio.

1.3 Outline of Thesis

The outline of the thesis is as follows:

Chapter 2 describes a comparative study of four channel modeling techniques including ray tracing, finite difference time domain (FDTD), event based transmission line matrix (TLM), and stochastic channel modeling used for understanding propagation environments. Chapter 3 performs experimental validation of existing Stochastic and TLM-based channel models with propagation measurements. Chapter 4 describes modeling techniques for simulating multipath parameters using TLM-based model. Chapter 5 demonstrates the application of channel modeling for improving QoS in communication systems. Chapter 6 draws conclusions for the work performed in this research.

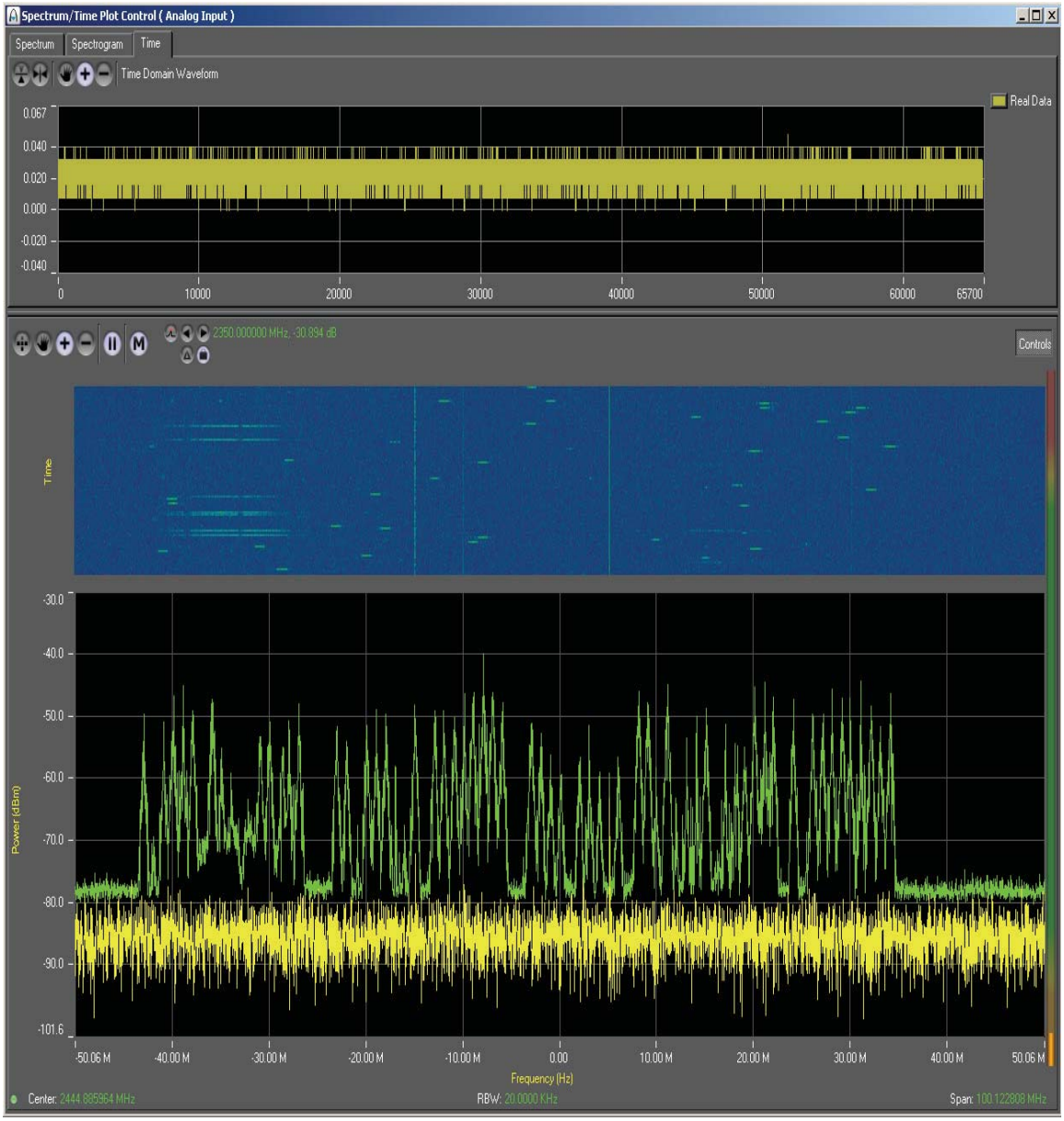

Figure 1.3: Ambient Channel Activity in a Plastics Plant

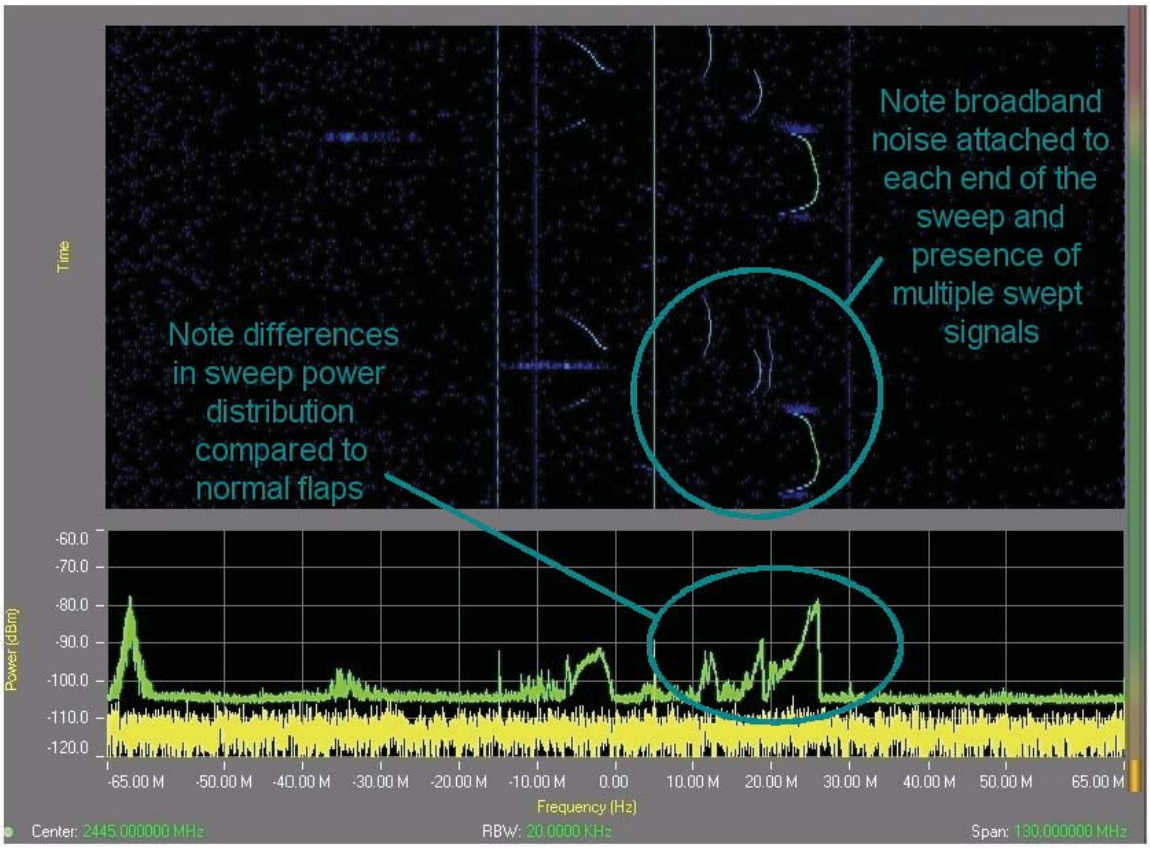

Figure 1.4: Ambient Noise Generated by a Jet Turbine Engine

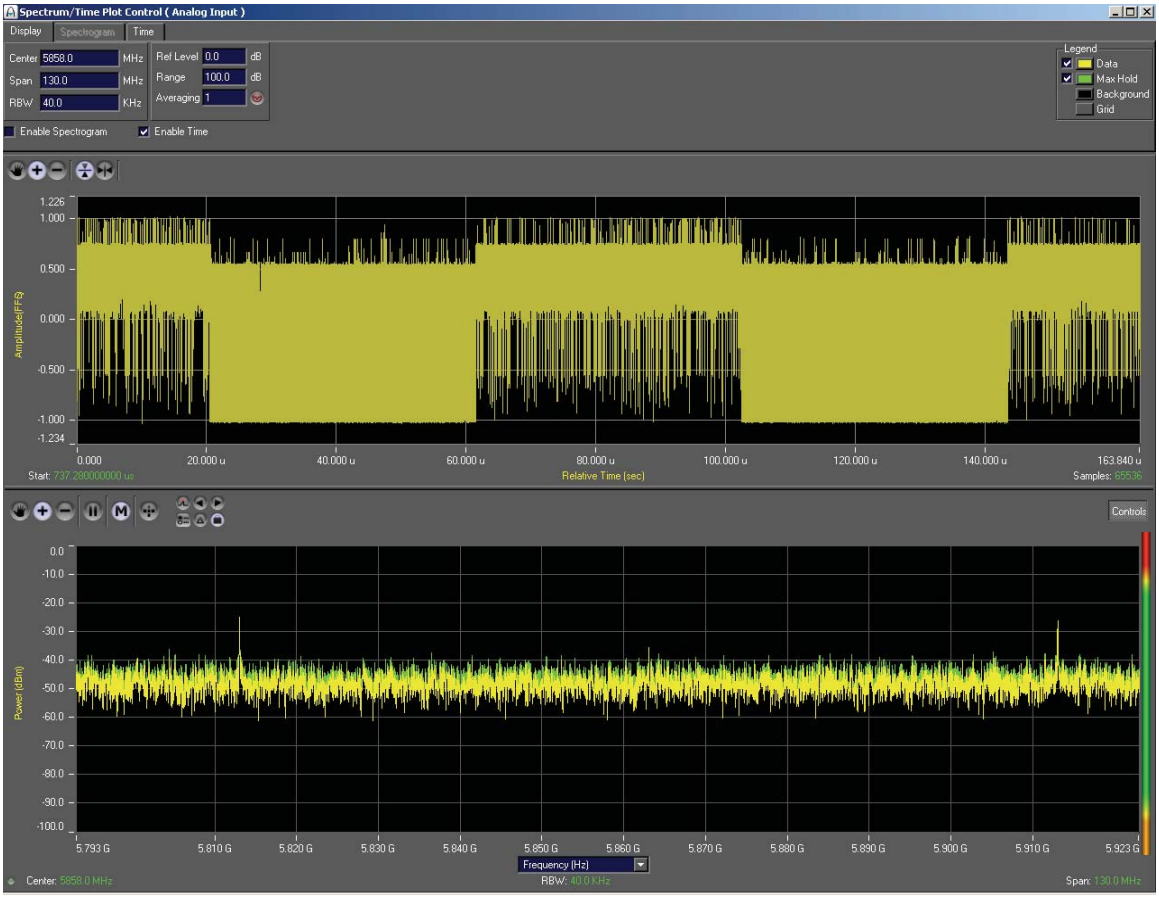

Figure 1.5: Ambient Noise Generated in a Coal Power Plant

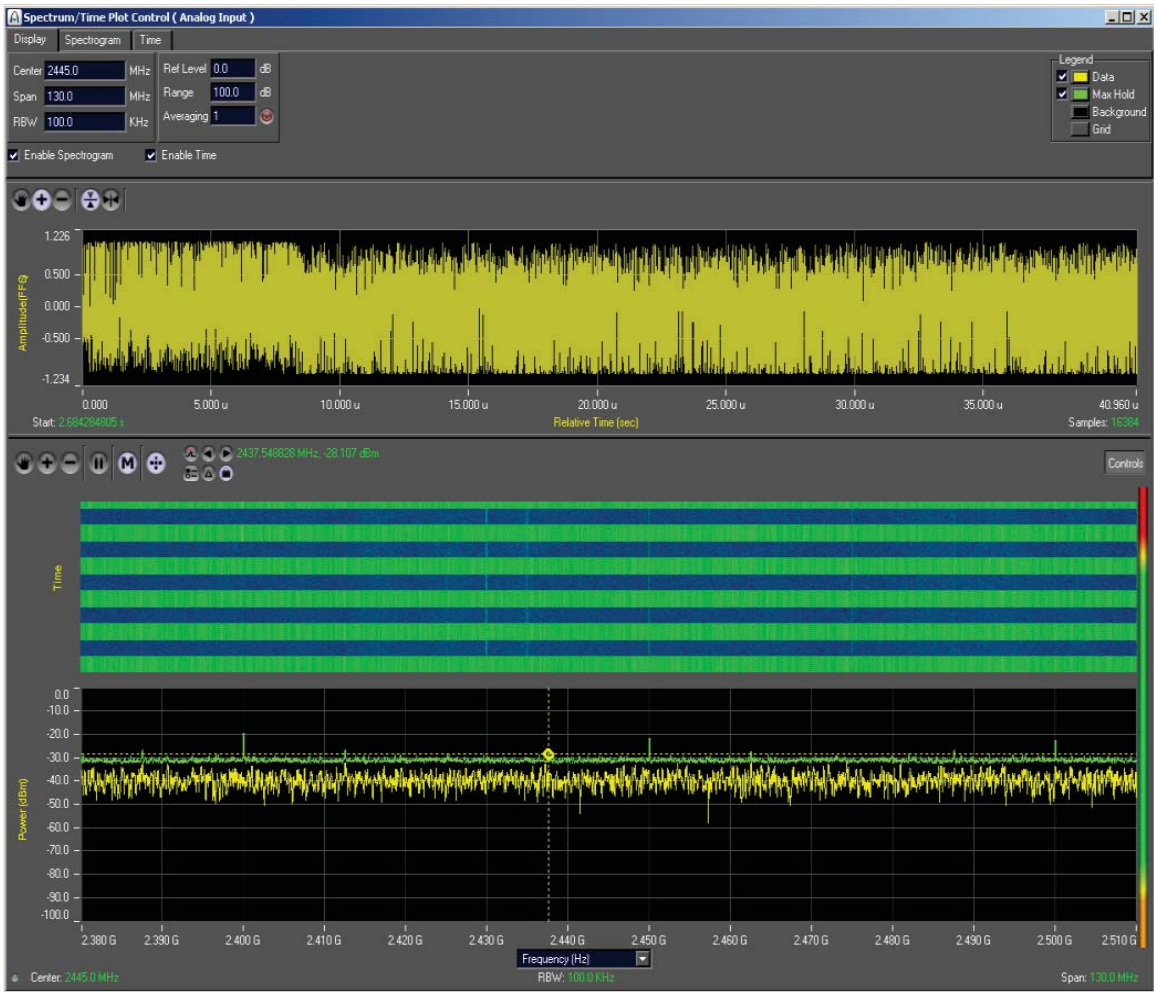

Figure 1.6: Ambient Noise Generated in a Steel Mini Mill

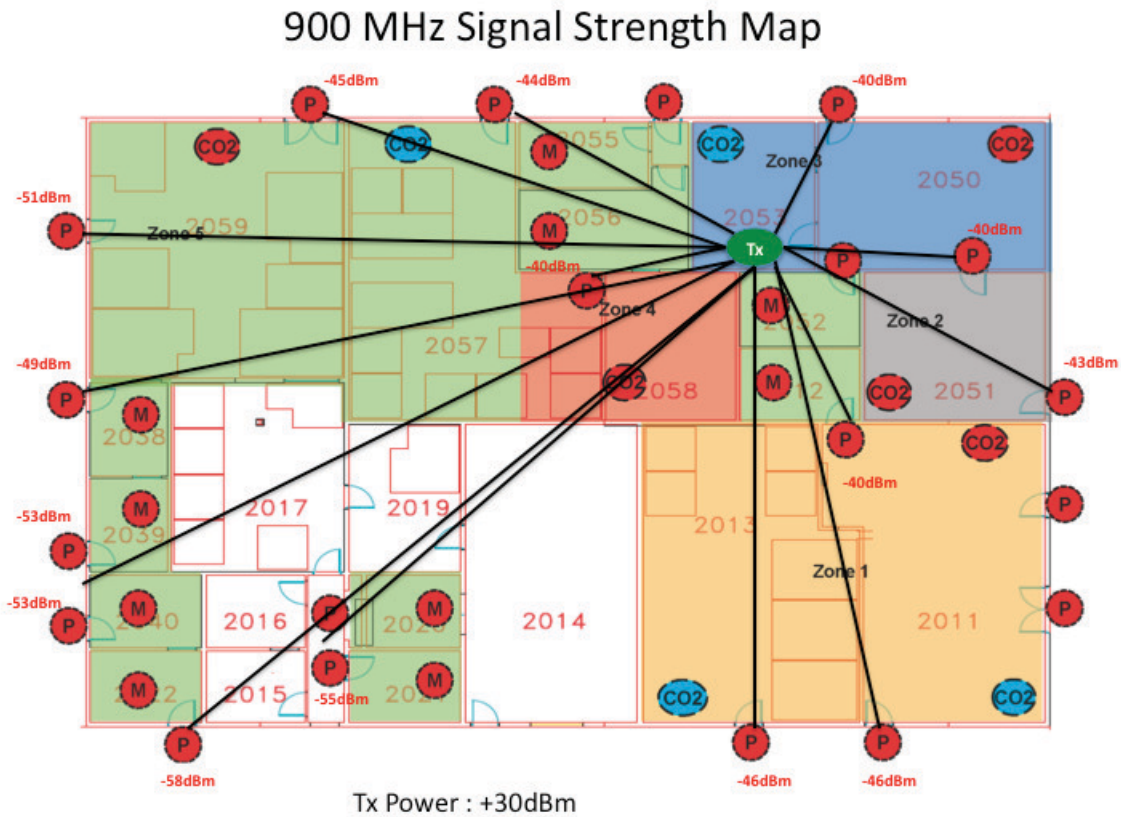

Figure 1.7: Attenuation of 900MHz Signal Inside a Building with TX Power 30dBm

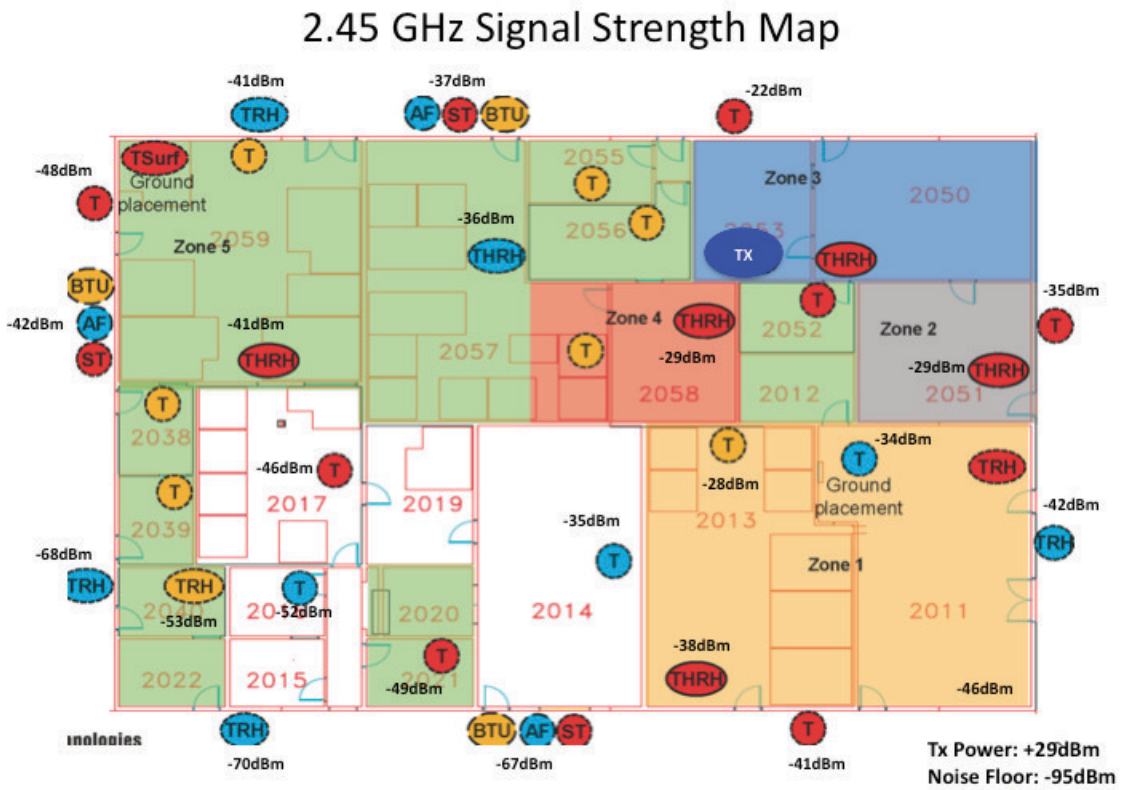

Figure 1.8: Attenuation of 2.4GHz Signal Inside a Building with TX Power 29dBm

Chapter 2

Comparative Study of Different Technologies

2.1 Introduction

Accurate radio channel models are essential for predicting the performance of wireless networks that operate in cluttered environments as shown in [8], [22], and [23]. Network performance in these types of environments is determined by interactions between the application traffic pattern, network protocol stack, and radio channel characteristics. Accurate performance predictions can only be obtained by accounting for all three of these elements, but radio channel characteristic is the key random variable in this context with limited to no radio designer control.

Network protocol simulation models, including those designed for modeling wireless networks, typically rely on empirical models of the physical radio channel. Empirical models are attractive because they are computationally cheap to use. This computational simplicity, however, comes at the cost of geometric simplicity that does not accurately represent the site-specific propagation characteristics

Empirical models are constructed in one of two ways. They can be based on simplifying assumptions concerning the physical geometry of the propagation space.

For example, free space propagation models assume that the radio wave propagates through empty space. Empirical models can also be constructed with a *best-fit* to experimental measurements obtained in a particular environment. For example, an equation can be constructed that approximates measured path loss as a function of distance, where the measured path loss data was obtained in an urban canyon. [43] [24] describes several empirical models of both types.

Physically based radio channel models are required to obtain site-specific predictions of radio channel behavior as shown in [46], [14], and [17]. There are two basic approaches to physical modeling of radio channels: ray tracing methods and finite difference methods. Ray tracing methods are based on the geometric theory of optics, and are, in fact, closely related to the computer graphics technique of the same name. Finite difference methods, which can be broadly considered to include transmission line matrix and finite difference time domain techniques, are discrete approximations to Maxwell's equations that directly simulate the propagation of an electromagnetic wave.

Ray tracing and finite difference methods are computationally expensive. Finite difference techniques in their complete form [50] are widely regarded as being unsuitable for simulating wave propagation over large areas. However, simplifications that can be incorporated into transmission line matrix methods have allowed for relatively large scale path loss predictions to be computed [34]. Ray tracing techniques are relatively insensitive to the dimensions of the space under consideration, but they can scale poorly when the geometry is complex, there are a large number of radio receivers, or both.

A event driven variation of the transmission line matrix method is described in [36]. The event driven model is designed for use in cluttered environments comprising many objects that do not effectively transmit radio waves. The event driven model is executed on a three dimensional spatial grid, with grid points being updated only when the electric field amplitude at that point is sufficiently strong. This significantly reduces the computational effort needed to simulate areas in which the radio wave can

not penetrate large volumes of space. Moreover, because the method is grid based, the computational cost is independent of the number of receivers [46].

Attempts to integrate physically based radio propagation models into network protocol simulators have been described in [14] and [51]. Largely, these efforts attempt to compute path loss using ray tracing techniques, with FDTD methods being used in small areas where ray tracing does not provide accurate results. When considering large areas and very large numbers of receivers, this approach suffers from the same computational drawbacks as ray tracing techniques. The FDTD addition largely serves to improve accuracy in those areas were ray tracing is likely to give poor results.

This chapter describes various techniques of importance for simulation the behavior of propagation channels with specific application to wireless network deployment in cluttered wireless environments

2.2 Ray Tracing

Ray tracing models are based on the geometric theory of optics. The basic assumption is that high frequency waves can be closely approximated by a discrete number of rays emanating from the wave source. Associated with each ray is its power, which diminishes with distance according to some empirical model (frequently, a free space model is used). However, the distance travelled by the ray is determined directly from its path through a three dimensional geometric model. Calculating this path is the computationally difficult part of the ray tracing model.

Ray tracing begins with the generation of a single ray by the transmitter. The ray follows a straight line until it encounters a surface. At a surface, the ray can be split into new rays that describes different physical effects. Typically, these include reflection from the surface, transmission through the surface, and possibly diffraction around the sharp edge of a surface. Other effects can also be simulated as shown in [32], [53], and [16]. The ray tracing process terminates when the ray reaches

the receiver or some threshold criteria is met (e.g., after some distance travelled or number of reflections/transmissions/diffractions). This process is repeated typically until some predefined number of rays have found a path to the receiver or some number of rays have been attempted. At this point, the approximate signal characteristics of the ray channel can be computed.

The ray tracing technique has been shown to be accurate for a broad range of scenarios [53] and [51]. The computational costs, however, can be rather high [16]. The computational effort required to complete a ray tracing scenario grows as the number of surfaces, and hence number of ray intersection tests, grows. The computational effort also increases as the number of receivers is increased, since at least one ray is required for each possible receiver, and in practice the number of required rays is roughly proportionally to the number of receivers.

Ray tracing techniques also require accurate geometry description of the environment. For highly cluttered environments, as shown in Chapter 1, obtaining accurate geometry description is often times infeasible. This limitation makes it difficult to obtain site-specific propagation characteristics.

2.3 Finite Difference Time Domain (FDTD)

Finite difference time domain methods are a class of numerical techniques, which broadly includes transmission line matrix methods, for solving the time domain Maxwell's equations. The four equations are:

- Gauss's Law: Relationship between electric field and charge

$$\nabla . E = \frac{\rho}{\epsilon_0} \tag{2.1}$$

- Gauss's Law of Magnetism: Sum total magnetic flux is zero

$$\nabla . B = 0 \tag{2.2}$$

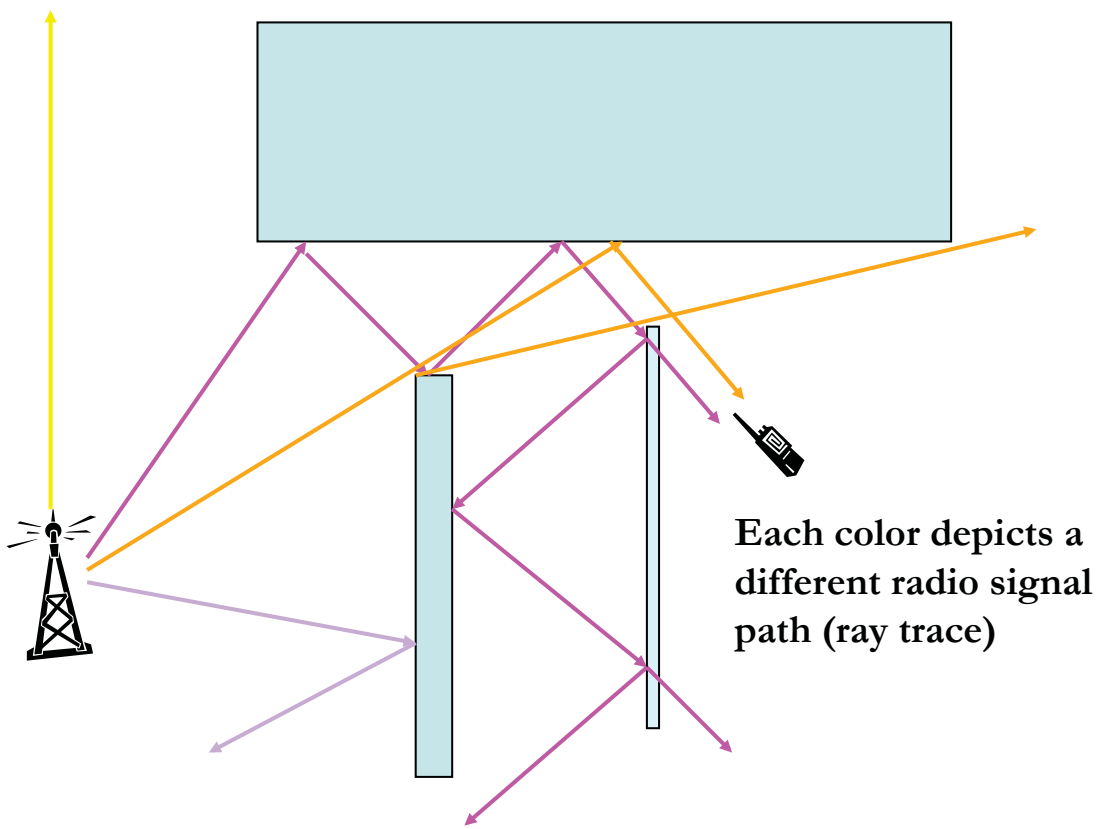

Figure 2.1: 2D Example of Ray Tracing

- Maxwell-Faraday Equation: Electromagnetic induction

$$\nabla \times E = -\frac{\partial B}{\partial t} \tag{2.3}$$

- Maxwell corrected Amperes Law: Changing electric field induces magnetic field and vice versa

$$\nabla \times B = \mu_0 J + \mu_0 \epsilon_0 \frac{\partial E}{\partial t} \tag{2.4}$$

where $\nabla.$ is the divergence operator, $\nabla\times$ is the curl operator, E is the electric field intensity, B is the magnetic flux density, ϵ_0 is the permittivity of the free space, μ_0 is the permeability of the free space, and J is the total current density.

Simpler schemes that are based on the linear wave equation and using low order numerical methods are generally preferred for radio wave propagation modeling. In their simplest form, finite difference methods approximate physical geometry with a three dimensional grid, and compute the field evolution at each grid point. In more complex models, a regular three dimensional grid is replaced with an irregular mesh that more accurately conforms to the shape of geometric features.

Finite difference methods, and related transmission line matrix methods, are grounded in well established physical laws, and as such can they can be applied to a very large class of problems. The computational effort needed to conduct a simulation is proportional to the number of grid points. For a three dimensional problem on a regular grid, the computational cost grows roughly as the third power of the grid resolution. The grid resolution is determined, in part, by the size of the space and, in part, by the type of information that is required. To compute, e.g., the impulse response of a radio channel requires a grid resolution that is much smaller than the signal wave length. Typically FDTD requires 10 cells per wavelength for effective simulation results.

2.4 Event Based Transmission Line Matrix (TLM)

The event driven TLM method is based on a simple model of radio wave propagation through a homogeneous, three dimensional space. This simple model is given by the linear wave equation

$$\frac{\partial^2}{\partial t^2}U(t,x,y,z) = c^2\left(\frac{\partial^2}{\partial x^2} + \frac{\partial^2}{\partial y^2} + \frac{\partial^2}{\partial z^2}\right)U(t,x,y,z) \tag{2.5}$$

where t is time, c is the propagation speed, x, y, and z are Cartesian spatial coordinates, and $U(t,x,y,z)$ is the scalar electric field potential at the space-time coordinate (t,x,y,z). A discrete approximation of this partial differential can be constructed using finite-differences. This finite difference approximation can be

viewed as a real valued cell space model [52]. This model can, in turn, be optimized for computation by reinterpreting it as a discrete event system [55]. The details of this transformation for the wave equation are given in [36] [37] [38].

In an inhomogeneous space, different wave-carrying mediums are modeled as described above. The different media are joined using reflection/transmission junctions that model reflection, transmission, and speed changes when a wave moves across the medium interface. A detailed description of the medium interface model can be found in [36] [38]. The resulting method is second order accurate within a homogeneous space, and first order accurate at material interfaces.

Two simplifications can be made without reducing the model's utility for predicting radio channel path loss. Both of these simplifications are based on the fact that the most useful portion of the radio signal is carried by the wave front that is moving through the air. This suggests, first, that waves traveling in other types of materials (e.g., concrete, earth) can be discarded. A simplified version of the reflection/transmission junction that only propagate reflected waves implements this simplification.

The second simplification restricts propagation calculations to the wave front by using two distinct cutoff thresholds. The first threshold is an *absolute* threshold, and a cell will not propagate any disturbance with a magnitude that is below this threshold. The second threshold is a *relative* threshold, and it defines a local cutoff threshold relative to the largest disturbance that has passed through the point. To be precise, let U_{max} be the largest signal amplitude observed at a point, y the junction output being considered, c_{abs} the absolute cutoff, and c_{rel} the relative cutoff. Then the output y will be propagated only if $y > c_{abs}$ and $y > U_{max} \cdot c_{rel}$.

If this model is simulated with a very coarse grid, then accurate path loss predictions can be made for receivers for which there is an open air (*not* free space) path to the transmitter. With a very fine grid, it is possible to construct the impulse response of the virtual radio channel between the transmitter and each individual grid point.

The computational cost of the event based TLM method are determined by the number of active grid points. If the propagation space is cluttered with objects that do not transmit radio signals, then the number of active grid points will be small when compared to the total number of grid points in the space. This can significantly reduce the computational complexity with respect to other finite difference techniques. Significantly, the accuracy of the method is similar to a complete low order finite difference technique and, as with other finite difference approaches, the signal characteristics are computed at every discrete grid point.

2.4.1 Equivalence of FDTD and TLM

The FDTD method is based on central difference approximations of Maxwells curl equations. The TLM method is based on a physical model of wave propagation. Both techniques are suitable for simulating Maxwell's equation in a given media. Literature exists demonstrating the formal equivalence of FDTD and TLM methods [12] [48]. These show that by using precise computer arithmetic, both methods would provide identical values at any time instant and at any location. The equivalence includes properties in terms of stability, energy conservation and flexibility in modeling irregular surfaces.

2.5 Dynamic Channel Modeling

While several techniques exist for modeling the propagation of electromagnetic waves as described in the sections above, there is a need for site-specific dynamic channel models [9]. These models are particularly useful for online estimation of the channel parameters and predicting the future states of the channel. Applications for such models include power control, adaptive antennae, and dynamic interference mitigation [42][31][41]. This includes system identification which is a process of constructing a mathematical model for a dynamic system from observations and prior knowledge.

2.5.1 State Space Model

State space models are widely used to model control systems and communication channels [11]. A state space model of a wireless channel has the form:

$$\begin{aligned} x_{t+1} &= A_t x_t + B_t w_t \\ y_t &= C_t x_t + D_t v_t \end{aligned} \tag{2.6}$$

where $x_t \in \Re^n$ is the state vector, $y_t \in \Re^d$ is a measurement vector sampled at the output of the channel, $w_t \in \Re^m$ is a state noise, and $v_t \in \Re^d$ is measurement noise. Channel parameters $\theta = \{A_t, B_t, C_t, D_t\}$ and states $\{x_t\}_t$, are the unknown parameters of the channel and shall be estimated using measurement data $\{y_t\}$. A_t is the state matrix, B_t denotes the process noise matrix, C_t denotes the output matrix, and D_t denotes the measurement noise matrix. The time varying property of the parameters adapts dynamically to the variety of outputs. Figure 2.2 shows the block diagram of relationship between the parameters θ.The Gaussian noise terms w_t and v_t capture the uncertainties introduced at each time step. These properties make the use of state space models appropriate to capture the time-varying stochasticity of the wireless channels. Future states of the received signal can be estimated based on the previous states.

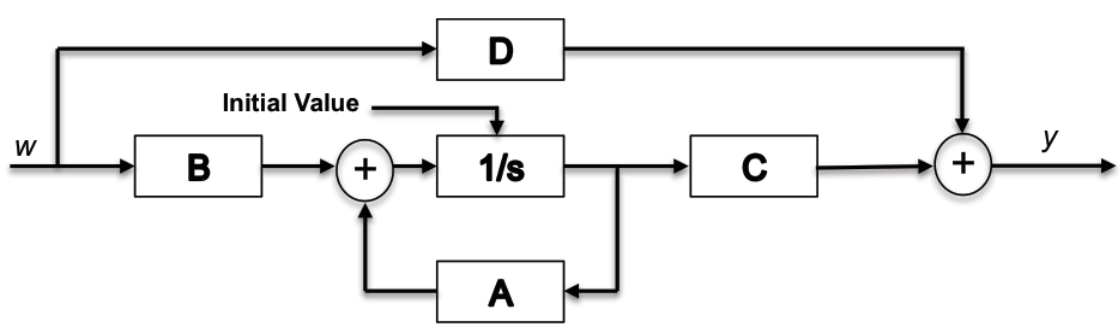

Figure 2.2: A Stochastic State Space Model

2.5.2 System Parameter Estimation

Channel parameters $\theta_t = \{A_t, B_t, C_t, D_t\}$ are estimated using Expectation-Maximization(EM) algorithm. The EM algorithm is an iterative numerical scheme to compute maximum likelihood estimates of the parameters given the measurement data Y_N. This is computed in two steps:

Step 1: This step evaluates the conditional expectation of the log-likelihood function given the complete data as

$$\Lambda(\theta, \theta_l) = E_{\theta_l}\{log\frac{dP_\theta}{dP_{\theta_l}}|y_T\} \tag{2.7}$$

Step 2: This step finds

$$\theta_{l+1} \in arg\ max_{\theta\in\Theta}\Lambda(\theta, \theta_l) \tag{2.8}$$

Step 1 and *Step 2* are repeated until the system parameters converge to the real parameters $\|\theta_l - \theta_{l-1}\| \leq \varepsilon$. P_0 denotes a fixed probability measure; and $\{P_{\theta_t}; \theta_t \in \Theta\}$ denotes a family of probability measures induced by the system parameters θ_t. If the original model is a white noise sequence, then $\{P_{\theta_t}; \theta_t \in \Theta\}$ is absolutely with respect to P_0. Moreover, it can be shown that under P_0 we have

$$P_0 = \begin{cases} x_{t+1} = w_t \\ y_t = v_t \end{cases} \tag{2.9}$$

The EM algorithm is described in [10][21] with the following equations:

$$\hat{A} = E\left(\sum_{t=1}^{N} \hat{x}_t\ \hat{x_{t-1}^T}\ |Y_N\right) \times \left[E\left(\sum_{t=1}^{N} \hat{x}_t\ \hat{x_t^T}\ |Y_N\right)\right]^{-1}$$

$$\hat{B^2} = \frac{1}{N}E\left(\sum_{t=1}^{N} (\hat{x}_t - A\hat{x_{t-1}})\,(\hat{x}_t - A\hat{x_{t-1}})^T\ |Y_N\right)$$

$$C = E\left(\sum_{t=1}^{N} \hat{y}_t\ \hat{x_t^T}\ |Y_N\right) \times \left[E\left(\sum_{t=1}^{N} \hat{x}_t\ \hat{x_t^T}\ |Y_N\right)\right]^{-1}$$

$$\hat{D}^2 = \frac{1}{N} E\left(\sum_{t=1}^{N} (\hat{y}_t - C\hat{x}_t)(\hat{y}_t - C\hat{x}_t)^T \ |Y_N\right) \tag{2.10}$$

$E(x)$ denotes the expectation operator to variable x, N denotes the total number of observed samples, an $\hat{x}_t$ denotes the estimated values at time t computed using the Kalman filter. The system 2.10 gives the EM parameter estimates at each iteration for the state space model. The advantage of the EM algorithm is that the parameter computation is less expensive than the Newton-Raphson method because the updated parameters at each iteration is linear. The system parameters can be computed from the conditional expectations [10]:

$$L_N^{(1)} = E\left\{\sum_{t=1}^{N} x_t^T Q x_t | Y_N\right\}$$

$$L_N^{(2)} = E\left\{\sum_{t=1}^{N} x_{t-1}^T Q x_{t-1} | Y_N\right\}$$

$$L_N^{(3)} = E\left\{\sum_{t=1}^{N} \left[x_t^T R x_{t-1} + x_{t-1}^T R^T x_t\right] | Y_N\right\}$$

$$L_N^{(4)} = E\left\{\sum_{t=1}^{N} \left[x_t^T S y_t + y_t^T S^T x_t\right] | Y_N\right\} \tag{2.11}$$

Where Q, R, S are defined by

$$Q = \left\{\frac{e_i e_j^T + e_j e_i^T}{2}; i, j = 1, 2, ..., m\right\}$$

$$R = \left\{\frac{e_i e_j^T}{2}; i, j = 1, 2, ..., m\right\}$$

$$S = \left\{\frac{e_i e_n^T}{2}; i, j = 1, 2, ...m; n = 1, 2, ...d\right\} \tag{2.12}$$

in which e_i is the unit vector in the Euclidean space; that is $e_t = 1$ in the ith position, and 0 elsewhere. consider the case when m=2, then

$$E\left(\sum_{t=1}^{N} \hat{x}_t \; \hat{x_{t-1}^T} \; |Y_N\right) = \begin{bmatrix} L_N^{(3)}(R_1 1) & L_N^{(3)}(R_2 1) \\ L_N^{(3)}(R_1 2) & L_N^{(3)}(R_2 2) \end{bmatrix} \tag{2.13}$$

The other terms in 2.10 can be computed similarly from 2.11.The filters defined in 2.11 can be obtained as derived in [21] as follows:

1) Filter estimate for $L_N^{(1)}$

$$\begin{aligned} L_N^{(1)} &= E\left\{\sum_{t=1}^{N} x_t^T Q x_t | Y_N\right\} \\ &= -\frac{1}{2} Tr\left(N_N^{(1)} P_{N|N}\right) - \frac{1}{2}\sum_{t=1}^{N} Tr\left(N_{t-1}^{(1)} \bar{P}_{t|t}\right) \\ &- \frac{1}{2}\sum_{t=1}^{N}[-2x_{t|t}^T P_{t|t}^{-1} r_t^{(1)} + 2x_{t|t-1}^T P_{t|t-1}^{-1} r_{t|t-1}^{(1)} \\ &- x_{t|t}^T N_t^{(1)} x_{t|t} + x_{t|t-1}^T B_{t-1}^{-2} A_{t-1} \bar{P}_{t|t} N_{t-1}^{(1)} \bar{P}_{t|t} A_{t-1}^T B_{t-1}^{-2} x_{t|t-1}] \end{aligned}$$

Where, $Tr(.)$ denotes the trace of the matrix, $r_t^{(1)}$ and $N_i^{(1)}$ satisfy the following recursions:

$$\begin{aligned} r_t^{(1)} &= \left(A_{t-1} - P_{t|t} C_{t-1}^T D_{t-1}^{-2} C_{t-1} A_{t-1}\right) r_{t-1}^{(1)} \\ &+ 2P_{t|t} Q x_{t|t-1} - P_{t|t} N_t^{(1)} P_{t|t} C_{t-1}^T D_{t-1}^{-2}\left(y_t - C_{t-1} x_{t|t-1}\right) \\ r_{t|t-1}^{(1)} &= A_{t-1} r_t^{(1)} \\ r_0^{(1)} &= 0_{m\times 1} \\ N_t^{(1)} &= B_{t-1}^{-2} A_{t-1} \bar{P}_{t|t} N_{t-1}^{(1)} \bar{P}_{t|t} A_{t-1}^T B_{t-1}^{-2} - 2Q \\ N_0^{(1)} &= 0_{m\times m} \end{aligned}$$

2) Filter estimate for $L_N^{(2)}$

$$\begin{aligned} L_N^{(2)} &= E\left\{\sum_{t=1}^{N} x_{t-1}^T Q x_{t-1} | Y_N\right\} \\ &= E_\theta\left\{x_0^T Q x_0 | Y_t\right\} + E_\theta\left\{\sum_{t=1}^{N} x_t^T Q x_t | Y_t\right\} \\ &- E_\theta\left\{x_N^T Q x_N | Y_N\right\} \end{aligned}$$

Therefore, $L_N^{(2)}$ can be obtained from filter $L_N^{(1)}$

3) Filter estimate for $L_N^{(3)}$

$$\begin{aligned} L_N^{(3)} &= E\left\{\sum_{t=1}^{N}\left(x_t^T R x_{t-1} + x_{t-1}^T R^T x_t\right)|Y_t\right\} \\ &- \frac{1}{2} Tr\left(N_N^{(3)} P_{N|N}\right) - \frac{1}{2}\sum_{t=1}^{N} Tr\left(N_{t-1}^{(3)} \bar{P}_{t|t}\right) \\ &- \frac{1}{2}\sum_{t=1}^{N}(-2x_{t|t}^T P_{t|t}^{-1} r_t^{(3)} + 2x_{t|t-1}^T P_{t|t-1}^{-1} r_{t|t-1}^{(3)} - x_{t|t}^T N_t^{(3)} x_{t|t} \\ &+ x_{t|t-1}^T B_{t-1}^{-2} A_{t-1} \bar{P}_{t|t} N_{t-1}^{(3)} \bar{P}_{t|t} A_{t-1}^T B_t^{-2} x_{t|t-1}) \end{aligned}$$

Where, $r_t^{(3)}$ and $N_t^{(3)}$ satisfy the following recursions

$$\begin{aligned} r_t^{(3)} &= \left(A_{t-1} - P_{t|t} C_{t-1}^T D_{t-1}^{-2} C_{t-1} A_{t-1}\right) r_{t-1}^{(3)} \\ &- P_{t|t} N_t^{(3)} P_{t|t} C_{t-1}^T D_{t-1}^{-2}\left(y_t - C_{t-1} x_{t|t-1}\right) \\ &+ \left(2P_{t|t} R + 2P_{t|t} B_{t-1}^{-2} A_{t-1} \bar{P}_{t|t} R^T A_{t-1}\right) x_{t-1|t-1} \\ r_{t|t-1}^{(3)} &= A_{t-1} r_t^{(3)} \\ r_0^{(3)} &= 0_{m\times 1} \\ N_t^{(3)} &= B_{t-1}^{-2} A_{t-1} \bar{P}_{t|t} N_{t-1}^{(3)} \bar{P}_{t|t} A_{t-1}^T B_{t-1}^{-2} \\ &- 2R\bar{P}_{t|t} A_{t-1}^T B_{t-1}^{-2} - 2B_{t-1}^{-2} A_{t-1} \bar{P}_{t|t} R^T \\ N_0^{(3)} &= 0_{m\times m} \end{aligned}$$

4) Filter estimate for $L_N^{(4)}$

$$\begin{aligned} L_N^{(4)} &= E\left\{\sum_{t=1}^{N}\left(x_t^T S y_t + y_t^T S^T x_t\right)|Y_t\right\} \\ &= \sum_{t=1}^{N}\left(x_{t|t}^T P_{t|t}^{-1} r_t^{(4)} - x_{t|t-1}^T P_{t|t-1}^{-1} r_{t|t-1}^{(4)}\right) \end{aligned}$$

Where $r_t^{(4)}$ satisfies the following recursions:

$$\begin{aligned} r_t^{(4)} &= \left(A_{t-1} - P_{t|t} C_{t-1}^T D_{t-1}^{-2} C_{t-1} A_{t-1}\right) r_{t-1}^{(4)} + 2P_{t|t} S y_t \\ r_{t|t-1}^{(4)} &= A_{t-1} r_t^{(4)} \\ r_0^{(4)} &= 0_{m\times 1} \end{aligned}$$

Using the filters for $L_N^{(i)}(i = 1, 2, 3, 4)$ and the Kalman filter described in the next section, the system parameters $\theta_t = \{A_t, B_t, C_t, D_t\}$ can the estimated through the EM algorithms.

2.5.3 System State Estimation

Given the system parameters θ_t and measurements $Y_t$the Kalman filter estimates the system state x_t. If w_k and v_k are assumed to be independent zero mean and unit variance Gaussian processes, then the Kalman filter estimates the state optimally in mean square sense and the filter-based EM algorithm yields a maximum likelihood (ML) parameter estimate. The Kalman filter can be described as follows [6]:

$$\hat{x_{t|t}} = A_{t-1}\hat{x_{t-1|t-1}} + P_{t|t} C_{t-1}^T D_{t-1}^{-2}\left(y_t \ - \ C_{t-1} A_{t-1} \hat{x_{t-1|t-1}}\right)$$

$$\hat{x_{t|t-1}} = A_{t-1} xt - \hat{1}|t-1$$

$$\hat{x_{0|0}} = m_0 \ t = 0, 1, 2, ...N \tag{2.14}$$

The sequence $P_{t|t}$, the estimate covariance, can also be given as the following [28]:

$$\bar{P}_{t|t}^{-1} = P_{t|t}^{-1} \ + \ A_{t-1}^{T} B_{t-1}^{-2} A_{t-1}$$

$$P_{t|t}^{-1} = C_{t-1}^{T} D_{t-1}^{-2} C \ + \ B_{t-1}^{-2} \ - B_{t-1}^{-2} \bar{P}_{t|t}^{-1} A_{t-1}^{T} B_{t-1}^{-2}$$

$$P_{t|t} = A_{t-1} P_{t-1|t-1} A_{t-1}^{T} \ + \ B_{t-1}^{2} \tag{2.15}$$

where $B^2{}_t = B_t B_t^T$, and $D_t^2 = D_t D_t^T$. $P_{t|t}$ and $\hat{x_{t|t}}$ can be computed recursively. Upon estimating the system parameters one-step prediction can be performed using Kalman filter as follows:

$$\hat{y_{t+1}} = \hat{C}_t \left(\hat{A}_t \hat{x_{t|t}} \ + \ \hat{K}_t \left(y_t \ - \ \hat{C}_t \hat{x_{t|t}} \right) \right) \tag{2.16}$$

where $\hat{y_{t+1}}$ is the predicted channel state at time $t+1$ and Kalman gain $\hat{K}_t$ is given by:

$$\hat{K}_t = \left(\hat{A_{t-1}} P_{t|t} \hat{C_{t-1}^T} \right) \left(\hat{C_{t-1}} P_{t|t} \hat{C_{t-1}^T} + \hat{D_{t-1}^2} \right) \tag{2.17}$$

2.6 Conclusion

Various different static and dynamic channel modeling techniques are explained in this chapter and compared for their computational efficiency. Different techniques are well suited for different applications. For example, wireless network deployment is primarily guided by received signal strength along with multipath characteristics of the channel. Measurement of channel characteristics at each network deployment is cost prohibitive. Simulation-based techniques that are computationally fast and accurate are needed for rapid deployment of wireless networks for various applications. In the following chapters validation of TLM and SDE-based techniques will be performed along with techniques for modeling the multipath characteristics of the channel along with application of the channel models.

Chapter 3

Model Validation

3.1 Introduction

Performing simulations of wireless channels involves choosing a tradeoff between higher accuracy (complex models, long simulation time) and lower compute time (simple models, lower accuracy). Ubiquitous use of wireless technology for various applications have shed a new light towards research into faster accurate channel models, particularly to assist in understanding the behavior of new generation of data protocols specific to applications. IEEE 802.11-based protocols, which are essentially ethernet packets-on-air, are identified as not optimal for various low-power,low-data rate wireless (sensor) networks. New channel models have to be validated against experimental data to understand their effectiveness. Validation of channel models can be divided into two major activities (1) performing validation in RF anechoic chambers to isolate interference from ambient RF sources, and (2) performing measurements in real-world environments. While anechoic chambers provide the luxury of fine-grained measurement instrumentation, [57] shows minimal advantages for practical purposes. Real-world measurements require careful understanding of the ambient RF conditions. Chapter 1 shows snapshots of the ambient RF environment. This chapter performs measurement-based validation of event-based TLM model and

compares the performance with ray-tracing and FDTD methods. A measurement-based validation of outdoor dynamic channel model is also performed.

3.2 Validation of Event-based TLM model

This section demonstrates by validation that the event driven transmission line matrix method described in [36] is suitable for generating large scale, site specific path loss databases for cluttered environments. The argument is based on a demonstration of the techniques computational efficiency and accuracy when compared to ray tracing and complete finite difference time domain methods. If these types of databases can be constructed quickly, then it would allow for accurate, site specific predictions of wireless network performance in cluttered environments.

3.2.1 Indoor Propagation

The accuracy and computation costs of these simulation methods were compared for a small, indoor propagation problem. This example problem is based on a laboratory room at Oak Ridge National Laboratory (ORNL). A transmitter was placed at one bench in this room, and signal strength measurements were taken at 90 locations on a bench at the opposite side of the room. These measurements are used as the basis for the accuracy comparison. A virtual reality modeling language (VRML) model of the room was constructed that describes its dimensions and large objects that might have a significant impact on the measured signal strength. The VRML model was constructed with one centimeter accuracy. Large objects, such as shelves and tables, were modeled, but small objects, such as bench equipment, were omitted.

Fig. 3.1 shows the floor plan of the room and the location of the 90 receivers and the transmitter. The transmitter (TX) is 80 cm from the edge of the bench on the right, and the 90 receivers (RXs) were set up on the opposite bench as indicated. The receivers were placed at 3.12 cm intervals. The first receiver was located 50 cm from

the bench edge. The dimensions of the room are 7.39 m x 7.39 m x 3.66 m. The wall is concrete and 25 cm thick. The table and benches consisted of wood and metal. Note that several small pieces of equipment were not included in the floor plan.

A pair of IEEE 802.15.4-based transceivers were used to obtain the experimental data. One node was configured as a transmitter and the other node as a receiver. The transmitter parameters were chosen as follows; 0 dBm transmitter power at 2405 MHz and vertically polarized antenna with 0 dB gain. The Receiver Signal Strength Indicator (RSSI) was used to measure the received signal strength.

Before taking measurements, the devices were calibrated in a shielded enclosure. One ZigBee transmitter and one receiver were placed in a small chamber made from

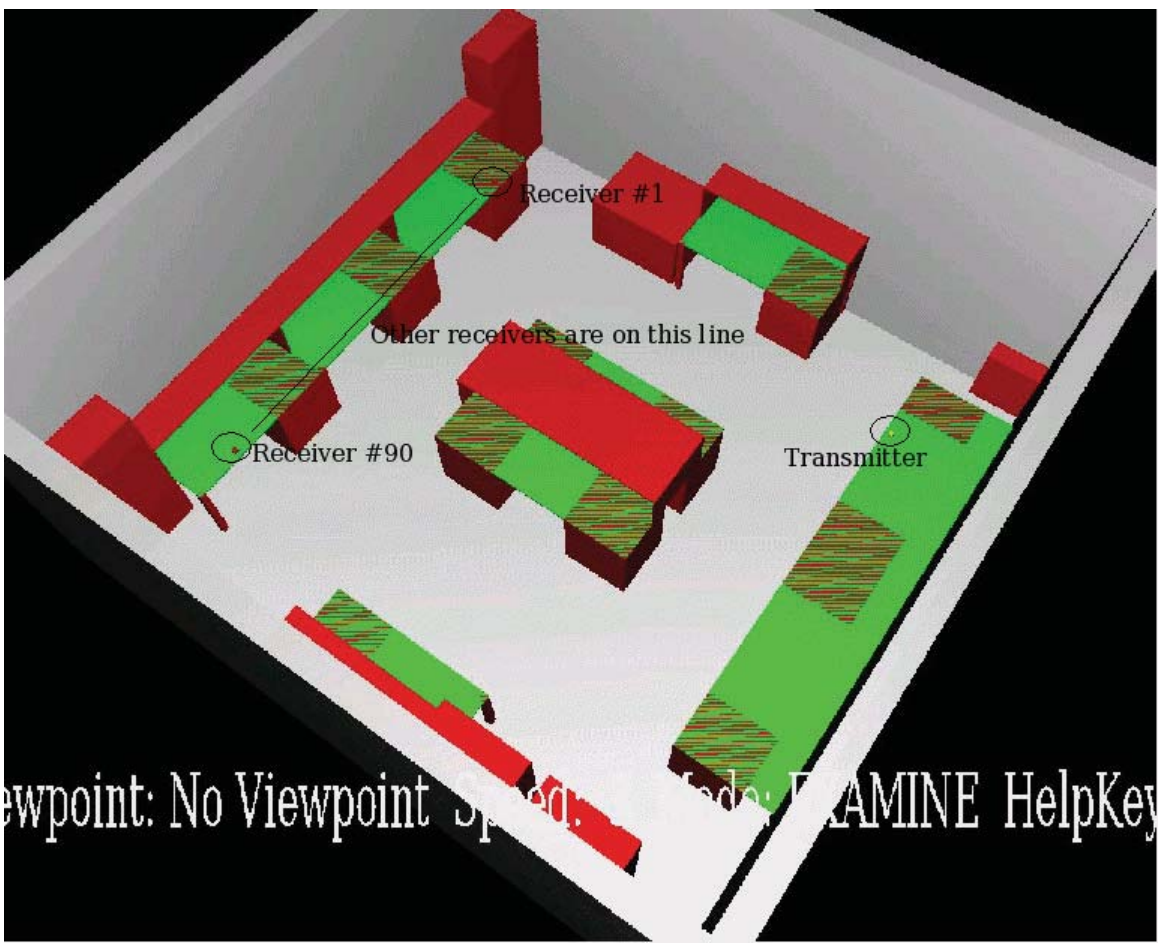

Figure 3.1: 3D View of the Room for the Validation Study

Eccosorb absorbing foam. Two calibration measurements were taken, one of which had transmitter and receiver separated by 20 cm, and the second at a distance of 30 cm. The measured RSSI value was 5 dB less than the expected path loss value, as calculated with the free space propagation equation, for the 20 cm case, and 7 dB less for 30 cm case. This indicates that the receiver power is actually 5 dB lower than the RSSI value.

To obtain the measurements, the transmitter was placed as shown in Fig. 3.1. The receiver was used to take measurements at 90 positions along the line shown in Fig. 3.1. Thirty packets with 50 byte payloads were transmitted for each of the 90 measurements, and the resulting RSSI values were recorded.

The VRML model for the room described above was used as input to three different radio channel modeling tools. Wireless Insite[45], a commercial ray tracing tool, was used as a representative example of available ray tracing software. XFDTD, from the same company that provides Wireless Insite, was used as an example of available finite difference tools. Our own event-based TLM simulator implements the TLM model.

Fig. 3.2 shows the measured path loss, path loss computed using Wireless Insite, and the path loss computed with the event based TLM simulators with different grid resolutions. The absolute and relative cutoff thresholds for the event based TLM model were set at 10^{-6} and 10^{-2}, respectively.

Fig. 3.3 shows the difference between the measured path loss and the path loss computed with Wireless Insite and the 10 cm resolution runs of the event driven TLM model. With a 10 cm grid resolution, all the methods provide accurate results with respect to measured path loss data.Figure 3.4 compares the measured and computed path-loss for the event based TLM simulation over a range of grid resolutions. The accuracy of the method is determined by the grid resolution, with more finely resolved grids giving better results. Fig. 3.5 and Fig. 3.6 show the 3D model used for FDTD simulation and the resulting field snapshot.

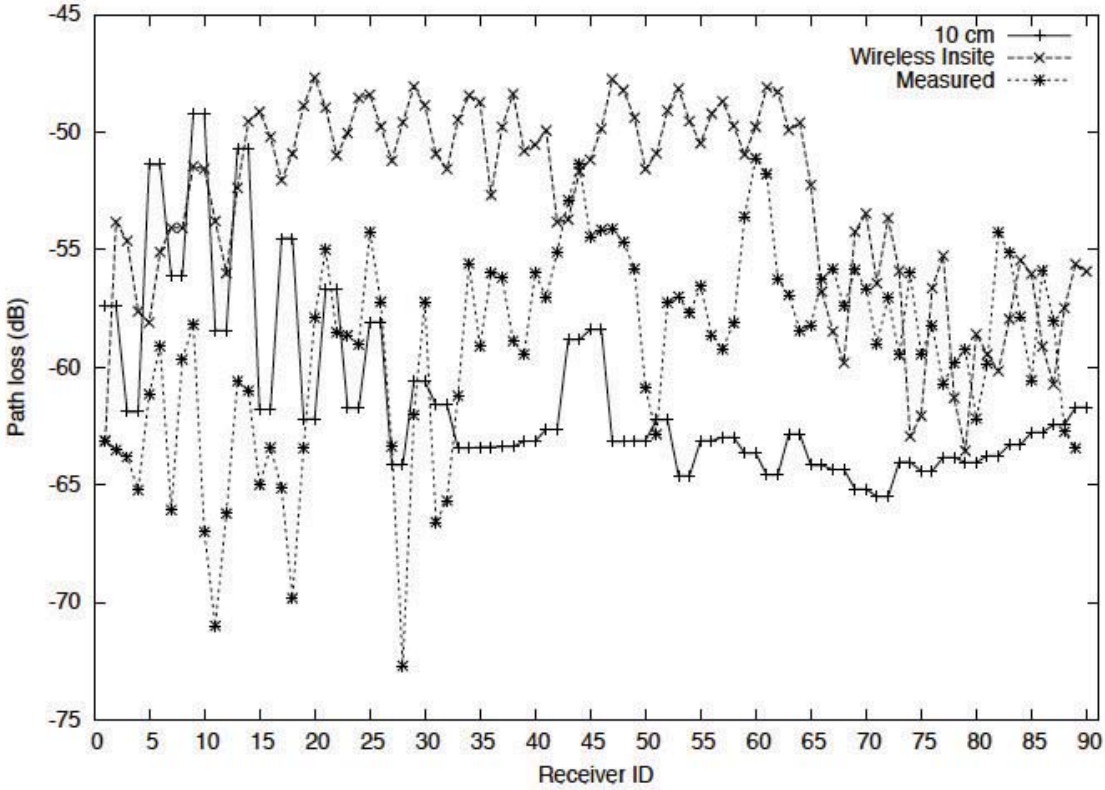

Figure 3.2: Measured and Simulated Path Loss as a Function of Receiver Location

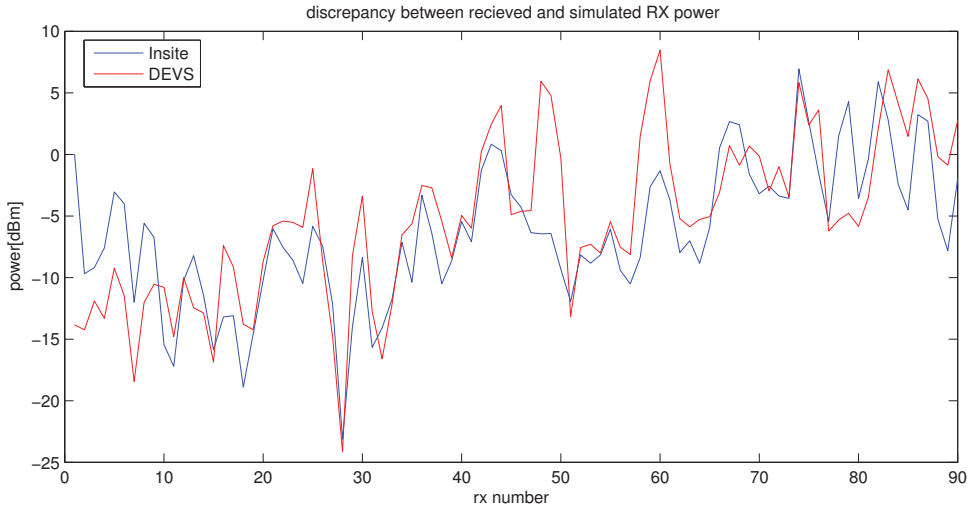

Figure 3.3: Error between Predicted and Measured Path Loss

For the event based TLM and XFDTD simulators, the model execution time increases as the grid resolution decreases. Fig. 3.7 shows the simulation completion time for the event based TLM and Ray Tracing software, including simulator initialization. These performance results were obtained using a 32-bit, 1.8 GHz Pentium 4 computer with 1.5 GB of RAM running the Windows operating system. Also included in this plot is the execution time of the Wireless Insite ray tracing simulation using the 90 receivers for which measurement data was available.

Fig. 3.8 shows the relationship between number of receivers in the simulation and the simulation time for each of the three simulation tools. Observe that as the number of receivers is increased, the ray-tracing simulation time increases. However, the XFDTD and event based TLM simulators have fixed execution times so long as the grid resolution is fixed. Note that the number of receiver positions for the XFDTD

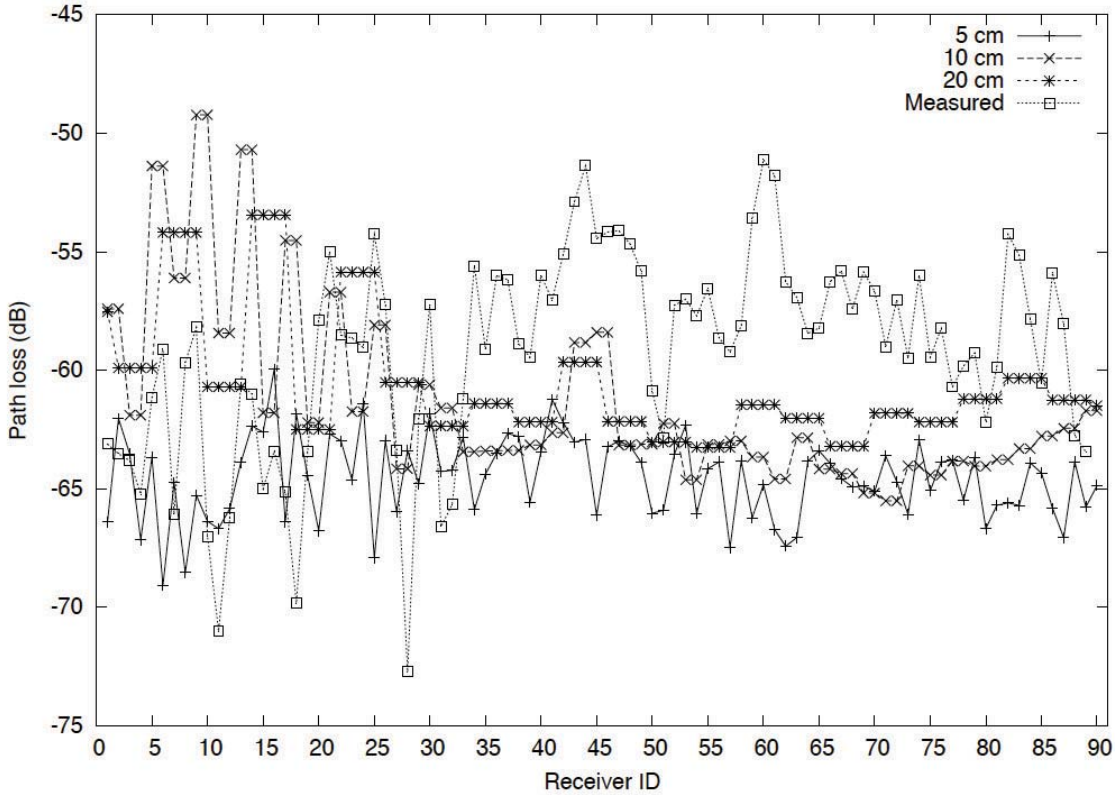

Figure 3.4: Comparison of Simulated and Measured Path Loss for Multiple Grid Resolution

and event based TML simulators is equal to the number of grid points, about 262,440 with a 10 cm grid resolution.

The event based TLM method is comparable in accuracy with commercial ray tracing and FDTD simulators. The accuracy of the simulations is validated using RF received power measurement. However, the execution times are not similar. In the case of ray tracing the execution time is linearly proportional to the number of nodes,

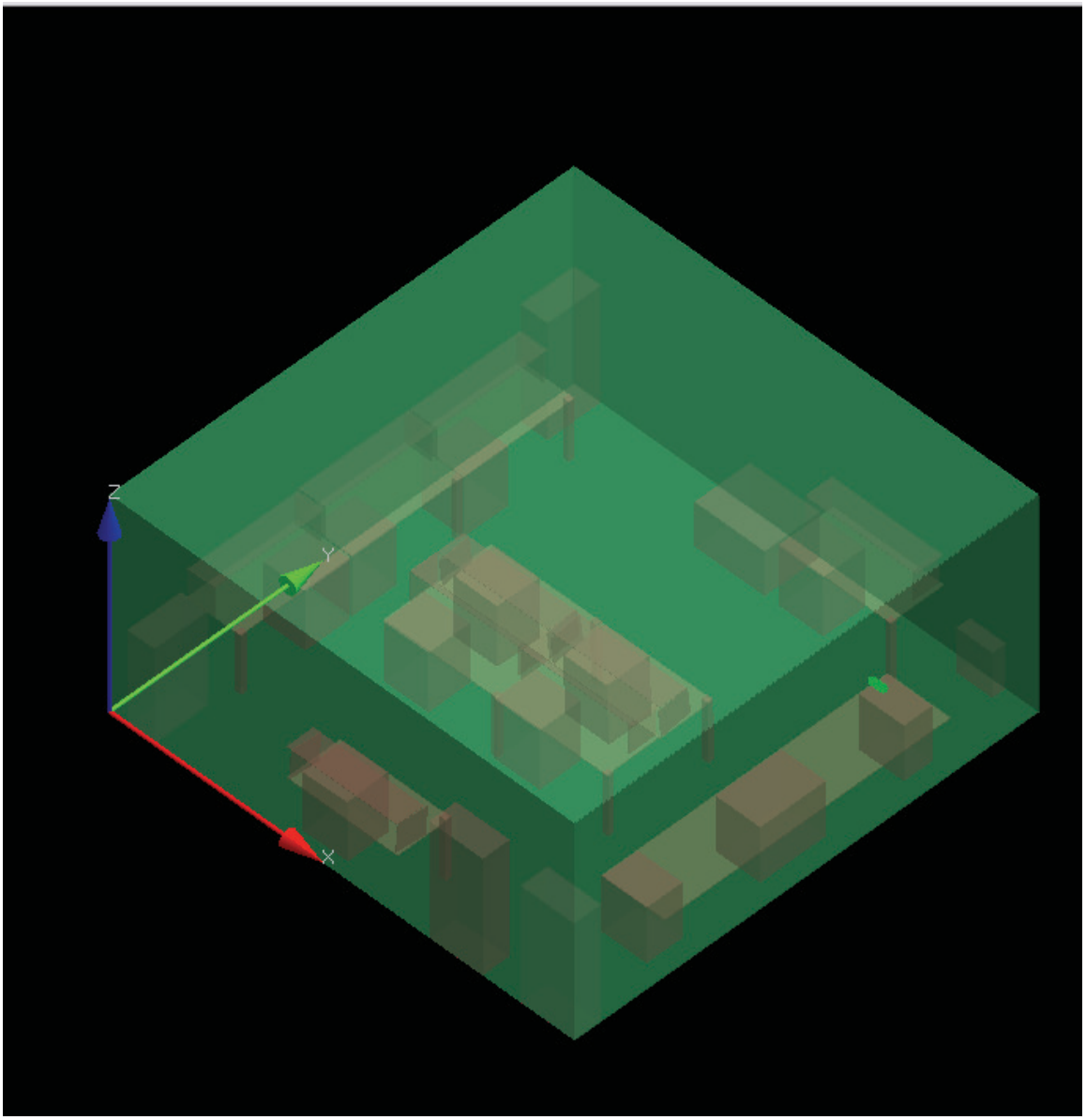

Figure 3.5: 3D Model for FDTD Simulation

the FDTD and TLM models are dependent on the grid size. The execution time of the TLM model is about 20,000 times less computationally intensive than FDTD technique for the same grid size and cutoff thresholds. Adaptive grid resolution is a topic of future research.

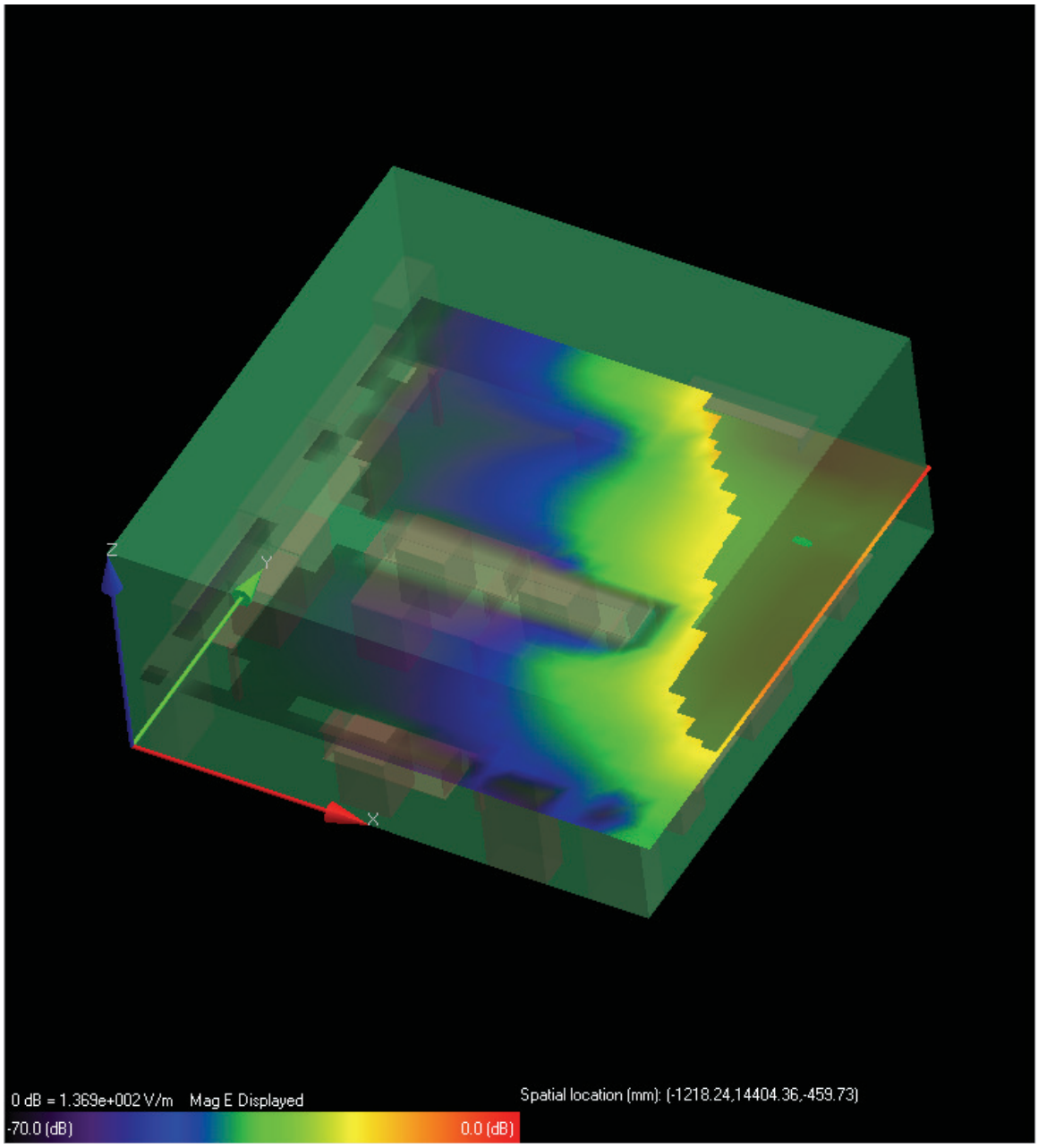

Figure 3.6: EM Field using FDTD Technique

The simulation completion time for the ray tracing, FDTD, and event based methods are shown in Table 3.1. These execution times include simulator initialization. The ray tracing simulation includes only the 90 receiver locations for which measurement data were obtained. Two of these simulation runs were done using a 1.8GHz Pentium 4 PC with 1.5GB RAM and running the Windows operating system the remainder were executed on a AMD Athlon(tm) 64 X2 Dual Core Processor 3800+ PC with 1GB RAM and running the Linux operating system.

Note that, while the 10cm event based simulation and ray tracing simulation require roughly the same amount of execution time, the event based simulation provides received signal power at every grid point. In contrast to this, the execution time of the ray tracing simulation is proportional to the number of receiver locations.

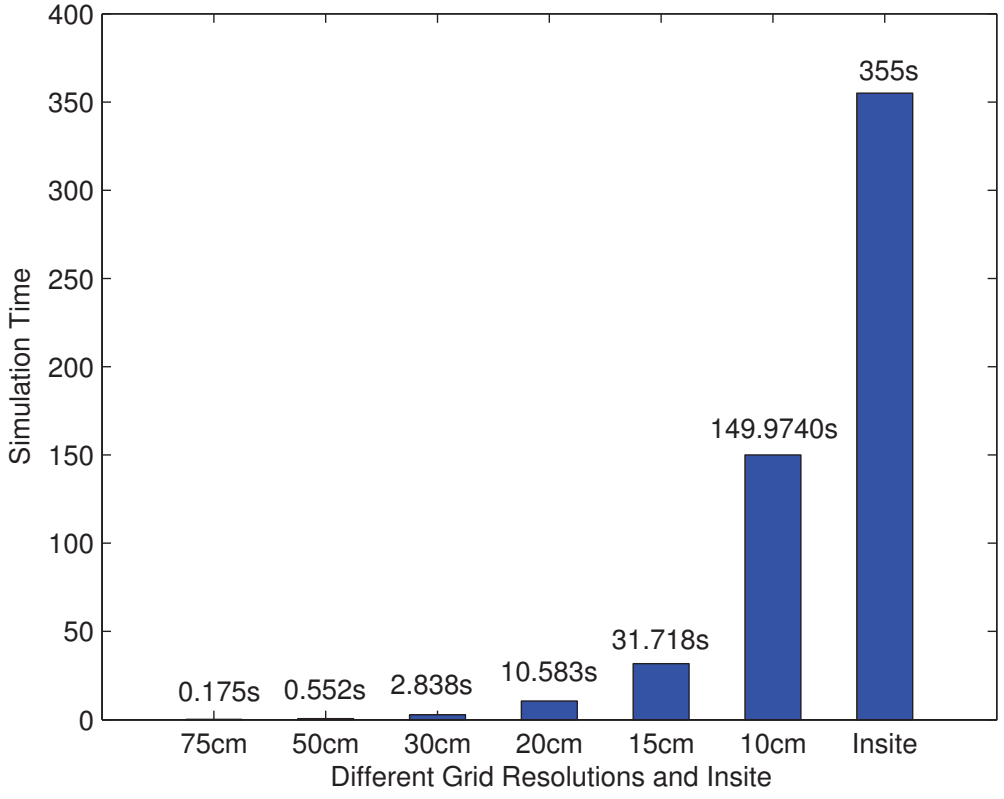

Figure 3.7: Execution Times for Multiple Grid Resolutions and Ray Tracing

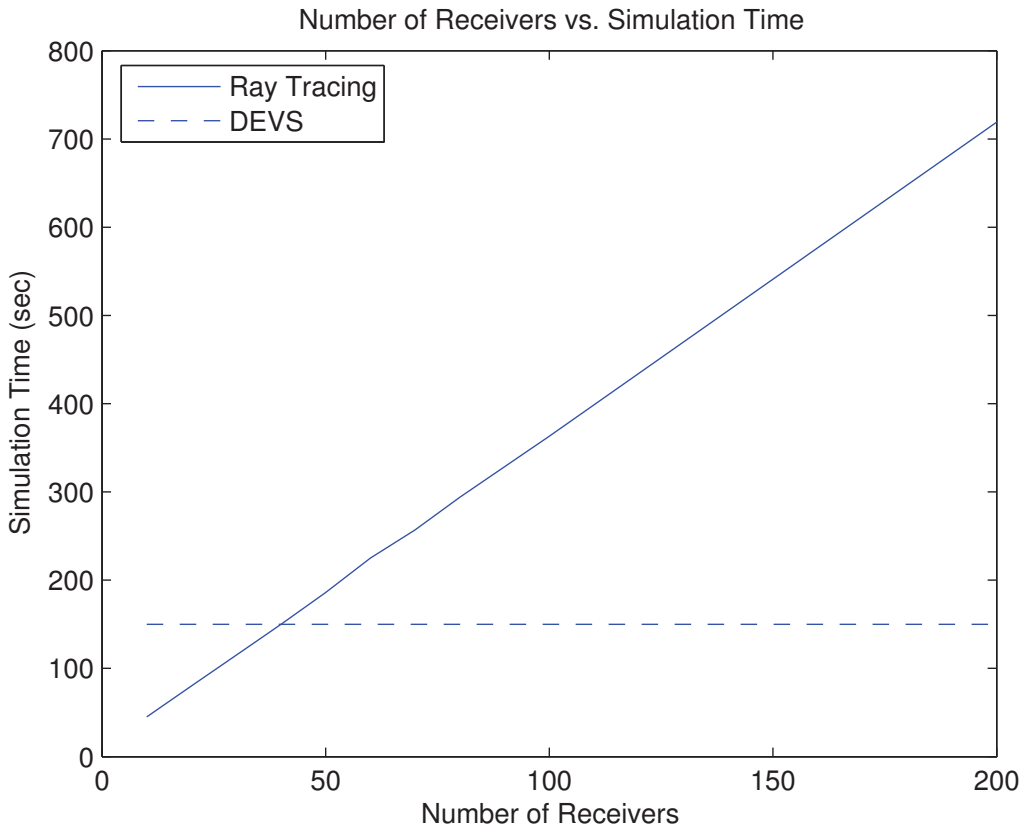

Figure 3.8: Simulation Time vs. Number of Receivers

This is clearly apparent in Fig. 7, which shows the execution time for the ray tracing simulation as new receiver locations are added.

Figure 3.8 illustrates the advantage of the proposed simulation scheme over ray tracing for use in mobile wireless network simulations. At 10cm, the simulation grid contains about 256,000 grid points. This corresponds to 256,000 potential receiver locations. Extrapolating from Fig. 7, obtaining path- loss data at 10cm resolution using the ray tracing method would require nearly 240 hours. In contrast, the event based TLM method needs only 5 minutes 13 seconds.

Model	Execution Time
Ray Tracing	4 minutes 55 seconds
Event based TLM	5 minutes 13 seconds
FDTD	14 hours 32 minutes 22 seconds

Table 3.1: Execution Times of Various Models

3.2.2 Outdoor Propagation

A second validation study was conducted in the visitors courtyard at Oak Ridge National Laboratory (ORNL). A three dimensional geometric model of the courtyard was obtained from the facilities management office at ORNL. This model describes the three key structures in the courtyard, but it does not model a slight elevation rise along the norther edge of the model. Ornamental building features, windows, a series of low stone pedestals, and the details of the road and other small objects at the northern edge of the courtyard are also neglected. Figure 3.9 shows the VRML model used in the simulation; Figure 3.10 shows a birds eye view of the courtyard. The simulation modeled the ground as clay, buildings as concrete, and a large glass section of the eastern most building (the section is shown in light gray) as glass. The clay, glass, and concrete were non-propagating.

Signal strength measurements were obtained at the receiver points indicated in Figure 3.9. The transmitter was placed near the entrance of the southern most building; its location is also shown in Figure 3.9. The height of the transmitter and every receiver except 8 was $1m$; 8 was $2m$ due to a set of steps at that location. Several received signal measurements, using a spectrum analyzer, were taken at each receiver point, and the minimum, maximum, and average values were recorded. In this instance, the transmitter power was 15 dBm at 900 MHz.

Two simulation runs were done, one using a grid resolution of 1m and the second with a grid resolution of 0.5m. The simulation was configured with cutoff parameters $v_c = 10^{-8}$ and $c_r = 10^{-3}$. Figure 3.11 shows simulated and measured path-loss data for this experiment. The simulated data closely follows the average measured

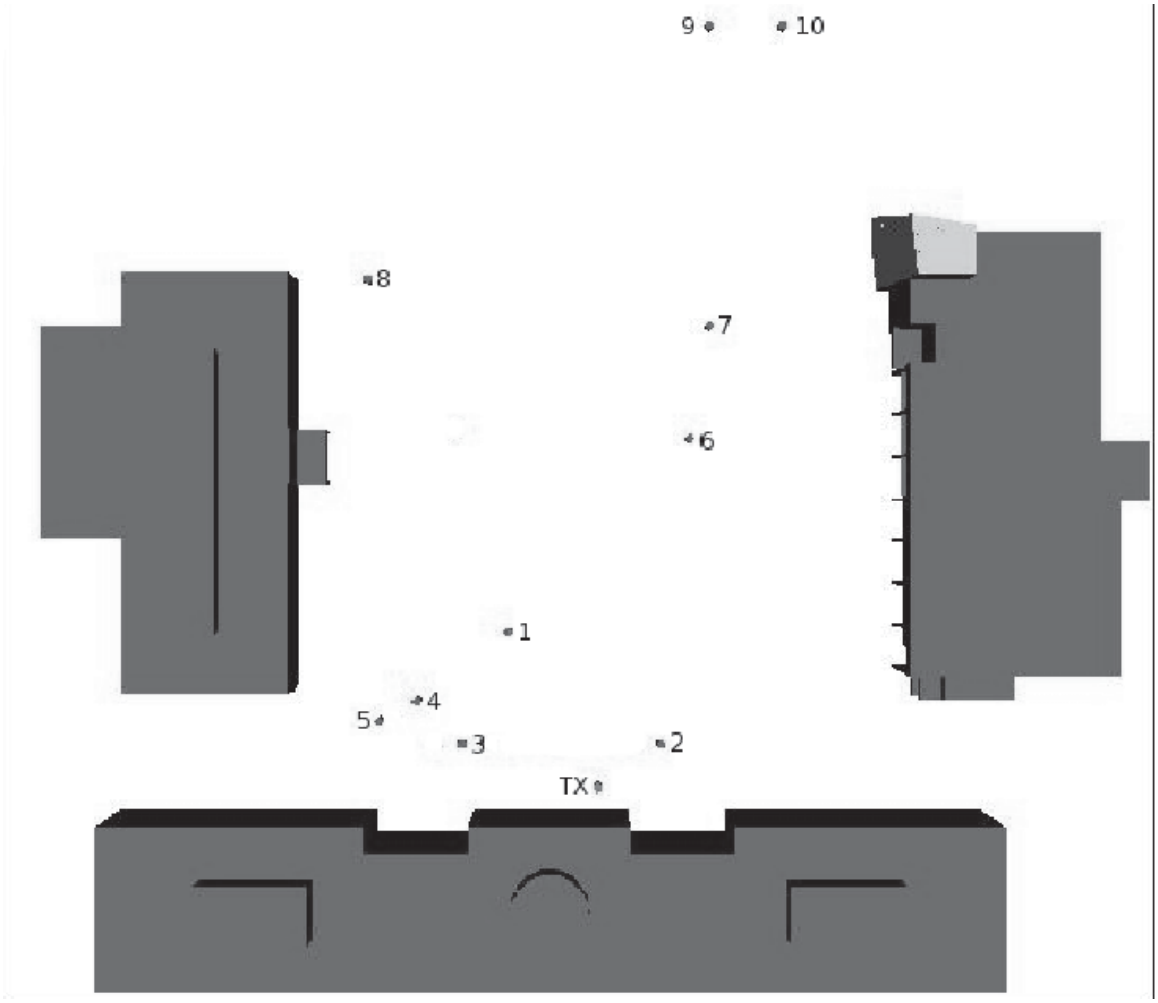

Figure 3.9: Top view of the courtyard with RX and TX locations used for study

received signal strength, and falls between the maximum and minimum received power measurements at every receiver location but 2. The agreement is reasonably accurate, but with a noticeable growth in the error for the farthest receivers. This increased error is likely due to a larger number of unaccounted for physical features at those locations. Also notice that the 0.5m simulation predicts a slightly smaller signal strength than the 1m resolution simulation.

Figure 3.10: Bird's Eye View of the Courtyard Used for Outdoor TLM Validation

3.3 Validation of SDE models

This section describes the validation of the dynamic channel models using SDEs as described in [40]. Outdoor wireless channels suffer from long term fading due to shadowing from buildings, vehicles, and terrain. The generalized spatio-temporal lognormal model in discrete time is given by:

$$\begin{aligned} x_{t+1} &= A_t x_t + B_t w_t \\ y_t &= s_t e^{k x_t} + D_t v_t \end{aligned} \tag{3.1}$$

where $s(t)$ is the information signal and k is the attenuation coefficient given by $-ln(10)/20$

3.3.1 Prediction

Kalman Filter

Upon estimating the system parameters one-step prediction can be performed using Kalman filter as follows:

$$\begin{aligned} y_{\hat{t+1}} &= e^{K\left(K\hat{A}_t x_{\hat{t|t}} + K\hat{G}_t\left(y_t - e^{Kx_{\hat{t|t}}}\right)\right)} \\ &+ \hat{D}_t\left(y_t - e^{Kx_{\hat{t|t}}}\right) \end{aligned} \tag{3.2}$$

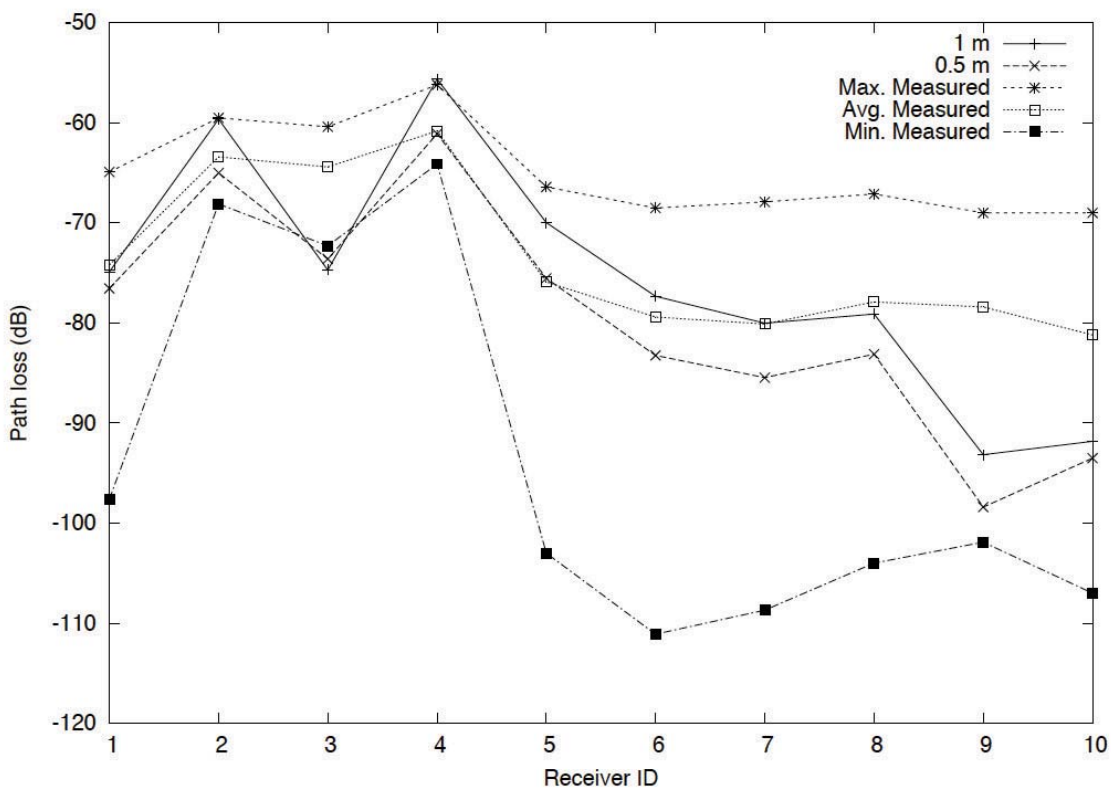

Figure 3.11: Comparison of the measurements and TLM simulations for outdoor TLM model

where $\hat{y_{t+1}}$ is the predicted channel state at time $t+1$ and Kalman gain $\hat{KG_t}$ is given by:

$$\hat{KG_t} = \left(\hat{A_{t-1}} P_{t|t} \hat{C_{t-1}^T}\right) \left(\hat{C_{t-1}} P_{t|t} \hat{C_{t-1}^T} + \hat{D_{t-1}^2}\right) \tag{3.3}$$

Prediction Error Minimization

Another technique for parameter estimation and prediction is prediction error minimization (PEM) [33]. The state space equation is written in the following form:

$$\begin{aligned} x_{t+1} &= A_t x_t + B_t e_t \\ y_t &= C_t x_t + e_t \end{aligned} \tag{3.4}$$

where e_t is the error between measured and predicted values. This algorithm minimizes the cost function defined as follows:

$$V_N = \sum_{t=1}^{N} {e_t}^T e_t \tag{3.5}$$

PEM uses the set of received measurements to estimate A_t, B_t, and C_t and repeats the process for each set of measurements. One-step prediction using PEM is computed using the following:

$$\hat{y_{t+1}} = \hat{C_t} \left(\hat{A_t}\hat{x_t} + \hat{B_t}\left(y_t - \hat{C_t}\hat{x_t}\right)\right) \tag{3.6}$$

where $\hat{y}_{t+1}$ is the predicted received signal strength at time $t+1$. $\hat{A}_t, \hat{B}_t$ and $\hat{C}_t$ are the estimated parameters and $\hat{x}_t$ is the estimated state at time t.

The channel parameters are estimated along with the path loss experienced by the signal using the received signal strength measurements from two datasets. The first data set was collected by driving through the ORNL campus and measuring a the signal strength from an antenna array transmitting at 5.8GHz as shown in Figure 3.12. Figure 3.13 shows the representation of the signal strength driving in

Figure 3.12: Transmitting Antenna on Top of a Building

the ORNL campus. Figure 3.14 shows the measured and estimated signal using EM and Kalman filter. The algorithm converges in less than 30 samples. The dataset includes over 1100 samples. The results demonstrate the effectiveness of the algorithm in tracking the statistics of the measured signal. However the algorithm over shoots during abrupt jumps of the signal. Figure 3.15 shows the error between measured and estimated signal. The average error is $\pm 2dBm$ with the peak error occurring at abrupt signal jumps at 15dBm.

Second dataset used is from SELECT Lab in Carnegie Mellon University [15]. This data expresses significant variation in received signal strength due to shadowing from downtown buildings and structures. The particular dataset used for this validation

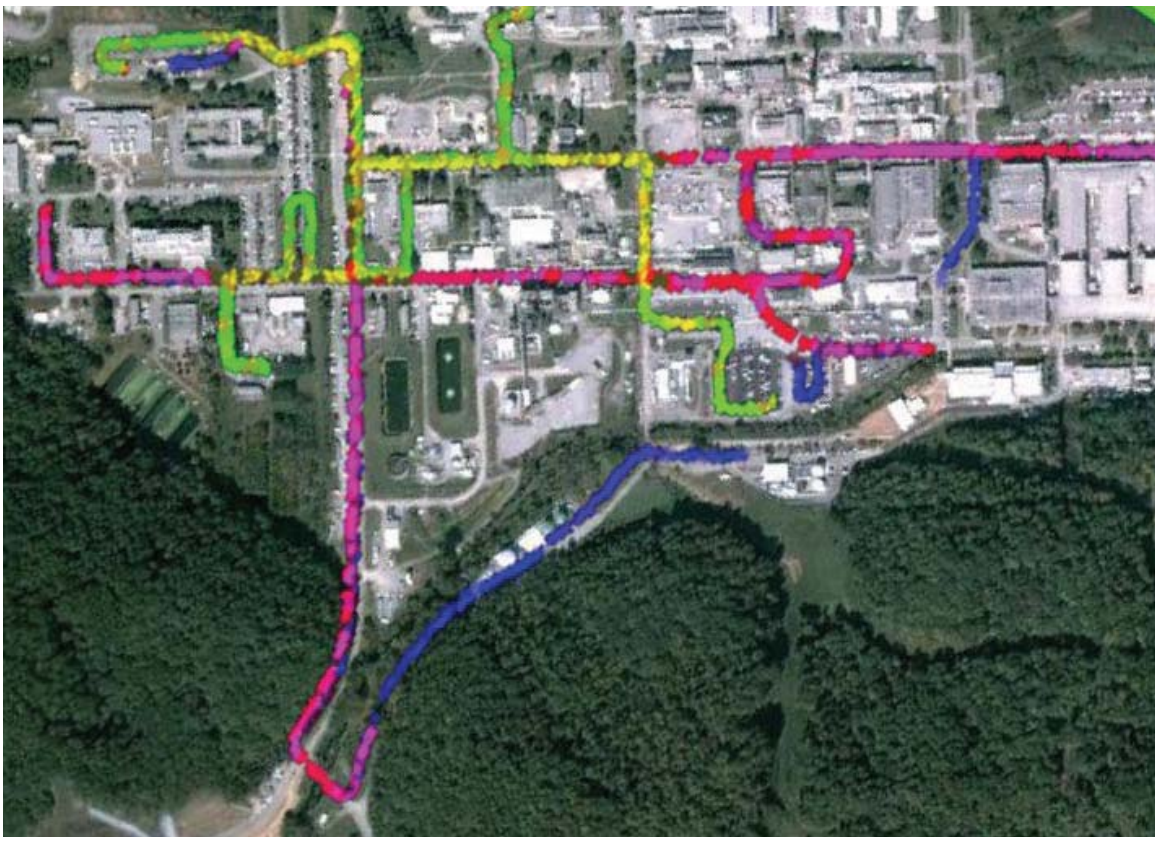

Figure 3.13: Received Signal Strength Measurement

belongs to the access point with MAC address $(00:0d:97:04:8e:0d)$. The receiver experiences loss of signal several times, thereby generating abrupt jumps in the measured signal. Figure 3.16 shows the comparison between measured and estimated signal using EM and Kalman filter. The dataset comprises of over 5500 samples. The algorithm converges in less than 20 samples. This data set has significant variation in signal strength and the algorithm captures the statistics of the signal with error as shown in figure 3.17. The average error is $\pm 6dBm$ and significant error during abrupt jumps. The EM and Kalman algorithm is proven to be adequate for all practical applications for performing state estimation of long-term fading.

Figure 3.18 represents the prediction using Kalman filter as described by equations 3.2 and 3.3. Figure 3.19 demonstrates the effectiveness of PEM algorithm as described in 3.6. The ORNL dataset is used to illustrate the effectiveness of the prediction

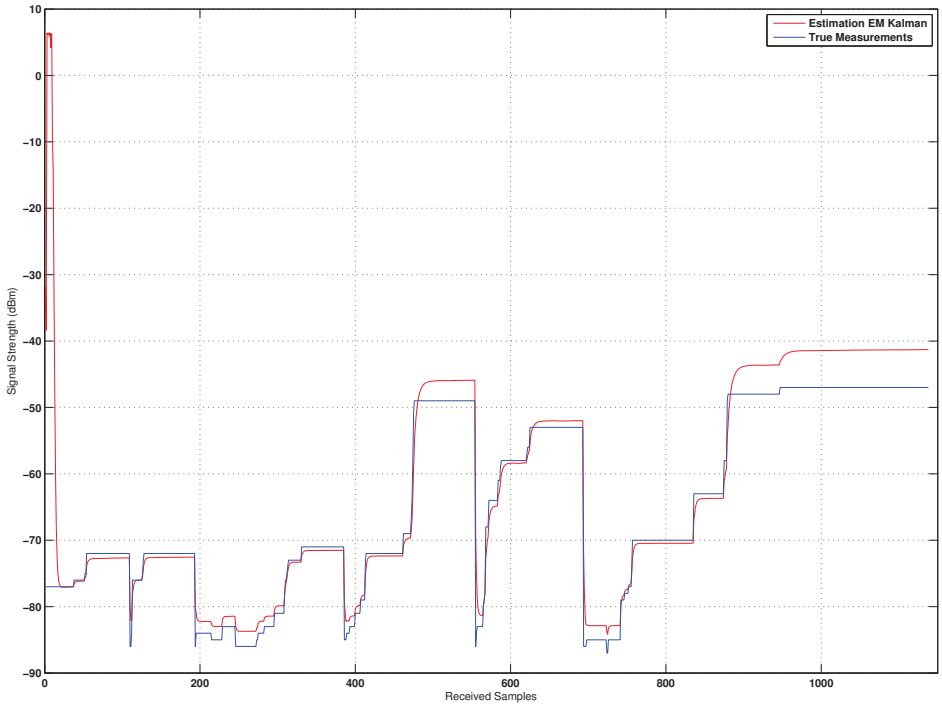

Figure 3.14: Measured and Estimated Values of ORNL data

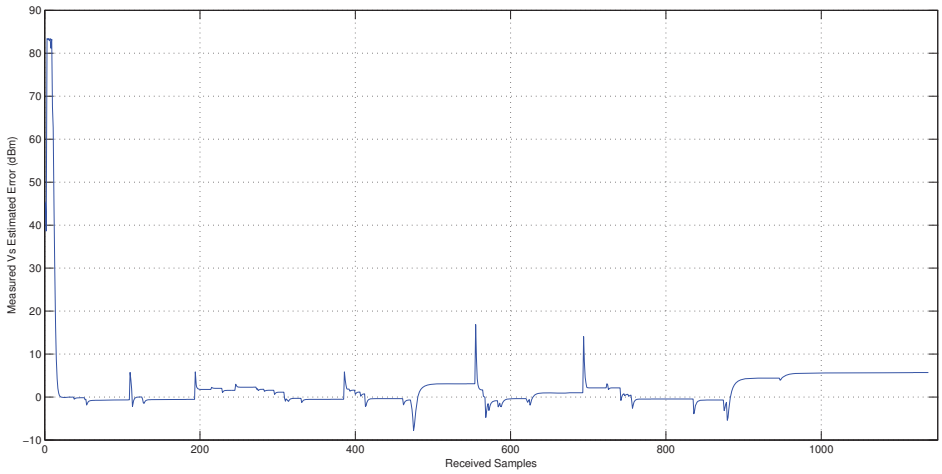

Figure 3.15: Error between Measured and Estimated Values of ORNL data

algorithms. The Kalman-based prediction takes about 30 samples to converge and predicts the statistics of the signal with minimal over shoot during abrupt signal

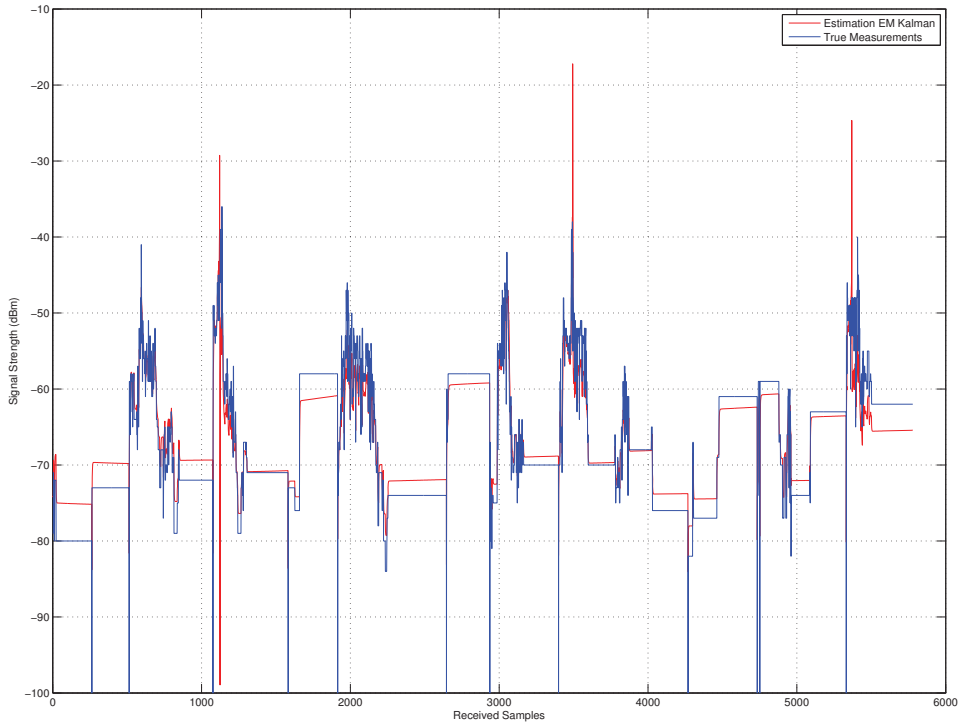

Figure 3.16: Measured and Estimated Values of WiFiPittsburgh data

changes. Figure 3.20 represents the error between measured and predicted signal using Kalman filter. The PEM-based prediction expresses minimal error but the algorithm over shoots and under shoots during abrupt jumps of the signal. Figure 3.21 shows the error between measured and predicted signal using PEM method. The experimental-based validation of the stochastic models demonstrated using numerical simulations illustrates the application of the models for designing modern communication infrastructure.

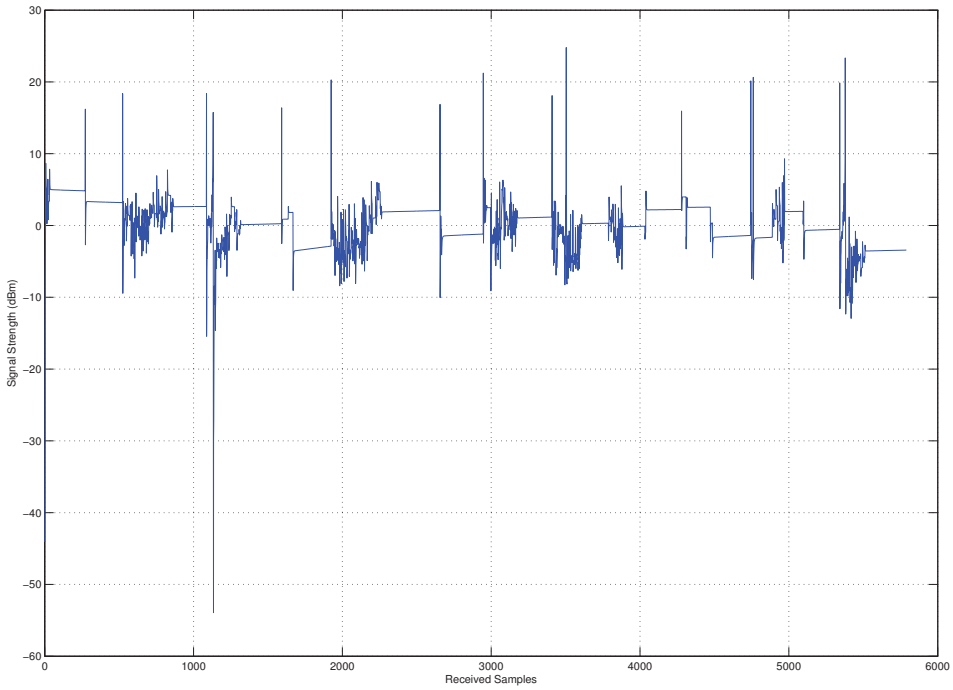

Figure 3.17: Error between Measured and Estimated Values of WiFiPittsburgh data

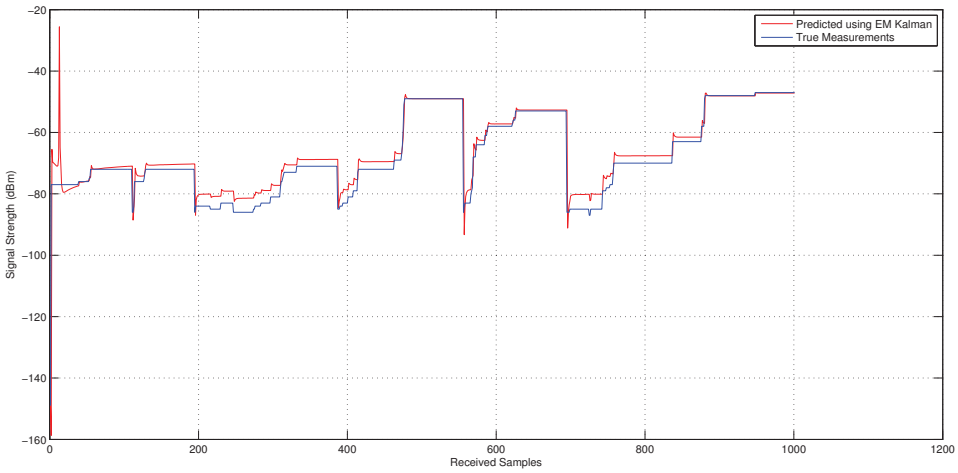

Figure 3.18: Prediction using EM Kalman and Measurement Values of ORNL data

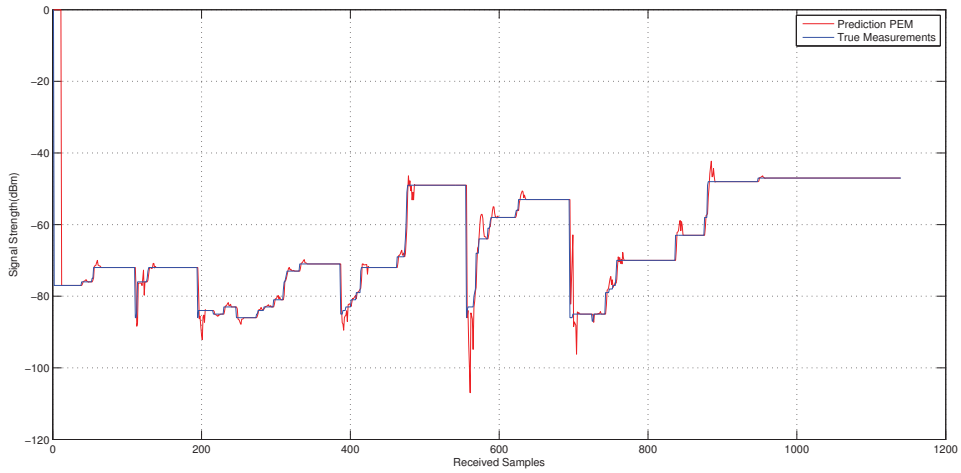

Figure 3.19: Prediction Using PEM and Measurement Values of ORNL Data

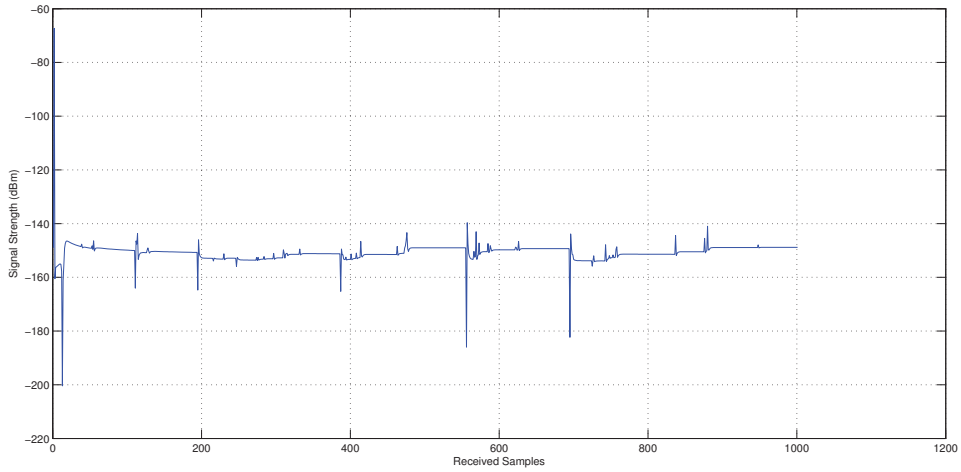

Figure 3.20: Error between Prediction Using KM and Measurement Values of ORNL Data

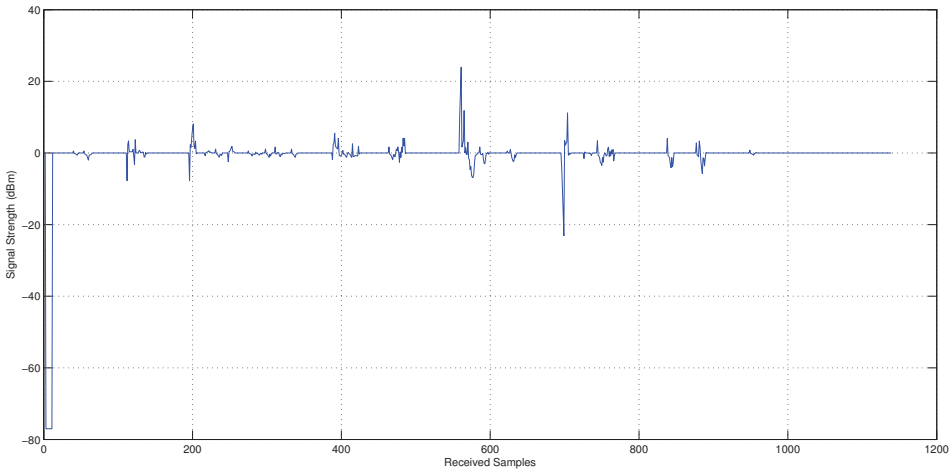

Figure 3.21: Error between Predicted Using PEM and Measured Values of ORNL Data

Chapter 4

Models for Multipath Propagation Characteristics

With the rapid growth in the networked environments for different industrial, scientific and defense applications, there is a vital need to assure the user or application a certain level of QoS. Environments like the industrial environment are particularly harsh with interference from metal structures (as found in the manufacturing sector), interference generated during wireless propagation, and multipath fading of the RF signal all invite novel mitigation techniques. The challenge of achieving benefits like improved energy efficiency using wireless is closely coupled with maintaining network QoS requirements. Assessment and management of QoS needs to occur, allowing the network to adapt to changes in the RF, information, and operational environments. The capacity to adapt is paramount to maintaining the required operational performance that is parameterized by throughput, latency, reliability and security. Key aspect of the radio communication is the propagation environment the transmitters and receivers reside.

Modeling techniques that perform pre-deployment validation of the environment performance measured by key parameters like received signal strength along with time and frequency dispersion characteristics of channel will provide information

for exploiting degrees of freedom in modulation schemes, antenna parameters, and transmit power. This chapter presents the use of event-based transmission line matrix method for performing computationally efficient modeling of indoor and outdoor propagation environments particularly to derive multipath characteristics of channel.

4.1 Multipath Characteristics

Indoor and outdoor radio channel typically has objects that continuously causes reflections from the structures that are large in size compared to the wavelength of transmission. This results in generating multiple versions of the signal at the receiver displaced with respect to one another in time and spatial orientation [43]. The multipath propagation results in signal smearing due to multiple copies of the transmitted signal and can result in inter-symbol interference. The received signal consists of a series of time-delayed and phase-shifted replicas of the transmitted signal resulting in a baseband channel impulse response is given by

$$h_b(t,\tau) = \sum_{i=0}^{N-1} a_i(t,\tau) exp[j(2\pi f_c \tau_i(t) + \phi_i(t,\tau))]\delta(\tau - \tau_i(t)) \tag{4.1}$$

Where $a_i(t,\tau)$ and $\tau_i(t)$ are the amplitudes and excess delays of the ith multipath component. τ represents the excess delay bin size used to create a uniformly discretized delay axis of power delay profile (PDP). The term $2\pi f_c \tau_i(t) + \phi_i(t,\tau)$ represents the phase-shift experienced by the signal. δ is the unit impulse function.

If the channel impulse response is assumed to be time invariant over small intervals of time then the channel impulse response [43] can be simplified as

$$h_b(\tau) = \sum_{i=0}^{N-1} a_i exp(-j\theta_i)\delta(\tau - \tau_i) \tag{4.2}$$

The PDP of the channel is obtained by taking the time average of the channel impulse response $|h_b(t;\tau)|^2$. As shown in [19] if the probing pulse $p(t) = \delta(t - \tau)$ has a time

duration that is much smaller than the channel impulse response, then $p(t)$ does not have to be deconvolved from the received signal $r(t) = h_(\tau) * p(t)$. In this case, the PDP is given by $|r(t;\tau)|^2$.

Delay spread characterizes the time-dispersive properties of the channel by defining the multipath density in the environment. It is simply the difference between the time of arrival of the first significant multipath component and the time of arrival of the next multipath component. This is usually obtained by observing the PDP in channel sounding experiments [43]. Three main parameters observed from the PDP are *mean excess delay, rms delay spread,* and *excess delay spread (X dB)*[43]. Mean excess delay,$\bar{\tau}$ is the first moment of the PDP and is defined by

$$\bar{\tau} = \frac{\sum_k P(\tau_k)\tau_k}{\sum_k P(\tau_k)} \tag{4.3}$$

τ_k represents delay of the kth multipath component. The RMS delay spread is the square root of the second central moment of the PDP and is defined by

$$\sigma_\tau = \sqrt{\bar{\tau^2} - (\bar{\tau})^2} \tag{4.4}$$

The maximum excess delay (X dB) of the PDP is the time delay during which the multipath energy falls to X dB below the maximum. The values of the three parameters depend on the choice of noise threshold used to process PDP $P(\tau)$. This threshold is used to differentiate between various received multipath components and thermal noise. If the noise threshold is too low, the noise may be processed as multipath, and the three parameters can be artificially high. The noise threshold is typically related to the receiver sensitivity of the communication device. Typical receiver sensitivities in IEEE 802.15.4 and IEEE 802.11 devices is $-95dBm$.

Measurement of delay spread is performed in two different ways[43]: (1) Direct RF Pulse System - This system transmits a narrowband pulse repetitively through a channel and a simple envelope detector is used to receive the signal along with a digital

storage oscilloscope. The local PDP can be observed by setting the oscilloscope in averaging mode; (2) Spread Spectrum Sliding Correlator - In this system the carrier signal is spread using a long pseudo-noise (PN) sequence and the received signal is filtered and despread using the same PN sequence. Maximum correlation peaks are tracked providing the PDP of the observed channel.

Measurement is not convenient and significantly time consuming when placing hundreds of wireless devices, for example, in an industrial plant. Most deployments need a fast and accurate method to estimate the channel parameters.

4.2 Transmission Line Matrix Method

The event-based transmission line matrix (TLM) method is based on a simple model of radio wave propagation through a homogeneous, three dimensional space. This simple model is given by the linear wave equation

$$\frac{\partial^2}{\partial t^2}U(t,x,y,z) = c^2\left(\frac{\partial^2}{\partial x^2} + \frac{\partial^2}{\partial y^2} + \frac{\partial^2}{\partial z^2}\right)U(t,x,y,z) \tag{4.5}$$

Where t is time, c is the propagation speed, x, y, and z are Cartesian spatial coordinates, and $U(t,x,y,z)$ is the scalar electric field potential at the space-time coordinate (t,x,y,z). A discrete approximation of this partial differential can be constructed using finite-differences. This finite difference approximation can be viewed as a real valued cell space model (see, e.g., [52]). This model can, in turn, be optimized for computation by reinterpreting it as a discrete event system (see, e.g., [55]). The details of this transformation for the wave equation are given in [36] [37] [38].

The fundamental computational element in this simulation is a simple junction structure that includes a variable for the state v of the junction and six input variables $v_1^+, v_2^+, v_3^+, v_4^+, v_5^+, v_6^+$ and six output variables $v_1^-, v_2^-, v_3^-, v_4^-, v_5^-, v_6^-$. The *state* and

output variables are computed by

$$v = \sum_{i=1}^{6} v_i^+ \tag{4.6}$$

$$v_i^- = \frac{v}{3} - v_i^+ \tag{4.7}$$

In an inhomogeneous space, different wave-carrying mediums are modeled as described above. The different media are joined using reflection and transmission junctions that model reflection, transmission, and speed changes when a wave moves across the medium interface. A detailed description of the medium interface model can be found in [36] [38]. The resulting method is second order accurate within a homogeneous space, and first order accurate at material interfaces.

The junctions are coupled to their neighbors using a memoryless function $z_{i,j}$ where i and j indicate opposite directions. Input to a junction i is computed using junction output y_i and neighboring junction output y_j. the resulting input is computed using

$$x_i = z_{i,j}(y_i, y_j) = Ry_i + Ty_j \tag{4.8}$$

Where R is the reflection coefficient and T is the transmission coefficient of the junction connection. If Z_i is the impedance of the junction generating output wave y_i and Z_j is the impedance of the junction generating output wave y_j, then the coefficients R and T are given by

$$R = \frac{Z_i - Z_j}{Z_i + Z_j} \tag{4.9}$$

$$T = \frac{2Z_j}{Z_i + Z_j} \tag{4.10}$$

Figure 4.1 shows the cubic 3D structure used for simulation. If this model is simulated with a very coarse grid, then accurate path loss predictions can be made for receivers for which there is an open air (*not* free space) path to the transmitter.

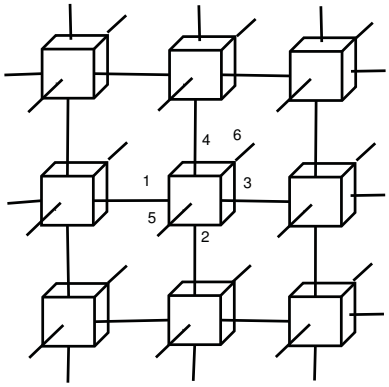

Figure 4.1: Junction Couplings Shown in a 2-D slice of a 3-D Mesh

With a very fine grid, it is possible to construct the impulse response of the virtual radio channel between the transmitter and each individual grid point.

The computational cost of the event-based TLM method are determined by the number of active grid points. If the propagation space is cluttered with objects that do not transmit radio signals, then the number of active grid points will be small when compared to the total number of grid points in the space. This can significantly reduce the computational complexity with respect to other grid-based simulation tools. Significantly, the accuracy of the method is similar to a complete low order finite difference technique and, as with other finite difference approaches, the signal characteristics are computed at every discrete grid point. Furthermore, the finite-difference methods are based on central difference approximations of Maxwells curl equations. The TLM method is based on a physical model of wave propagation. Both techniques are suitable for simulating Maxwell's equation in a given media. Literature exists demonstrating the formal equivalence of finite-difference time domain (FDTD) and TLM methods [12] [48] demonstrating that by using precise computer arithmetic, both methods would provide identical values at any time instant and at any location. The equivalence includes properties in terms of stability, energy conservation and flexibility in modeling irregular surfaces.

Figure 4.2 shows the excitation signal for obtaining the unit impulse response of the channel. A large air box is used for demonstrating the free space propagation

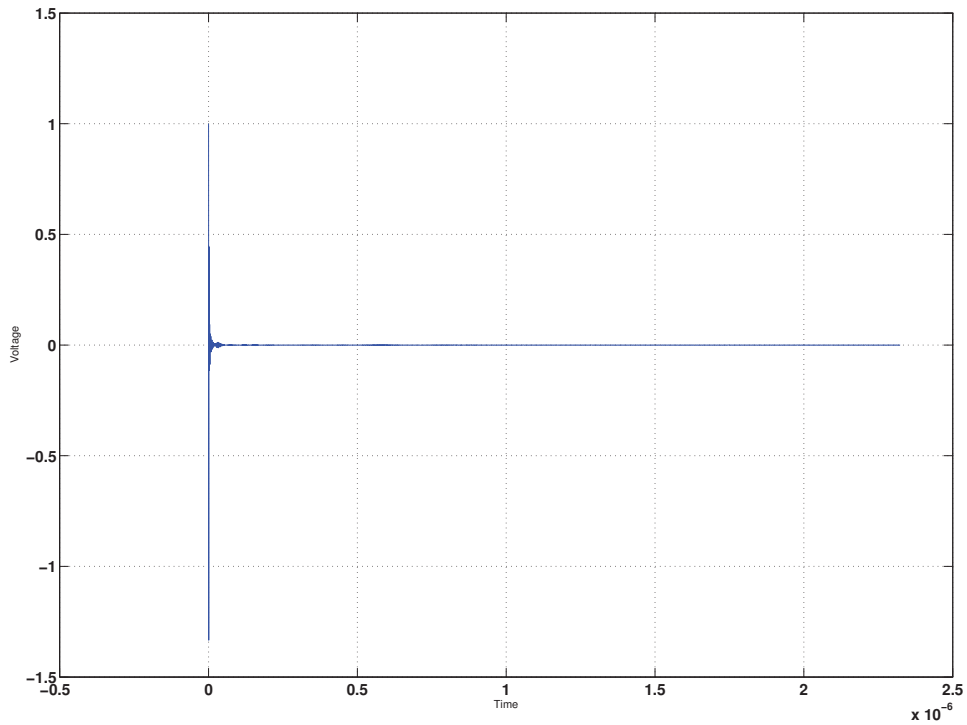

Figure 4.2: Excitation Pulse Used for TLM Simulation

modeling of the channel. Figure 4.3 shows the received signal or the impulse response of the channel. The TLM algorithm introduces a numerical decay of the signal due to partial voltages from neighboring scattering junctions. [25] elaborates the truncation and velocity errors in TLM-based wave propagation schemes and correction techniques.

The TLM method described above is excited with unit impulse and at each junction the signal is partly reflected and partly transmitted based on the junction impedance. At the measurement point we obtain a stream of pulses that arrive from six different directions. These approximate the impulse response of the channel.

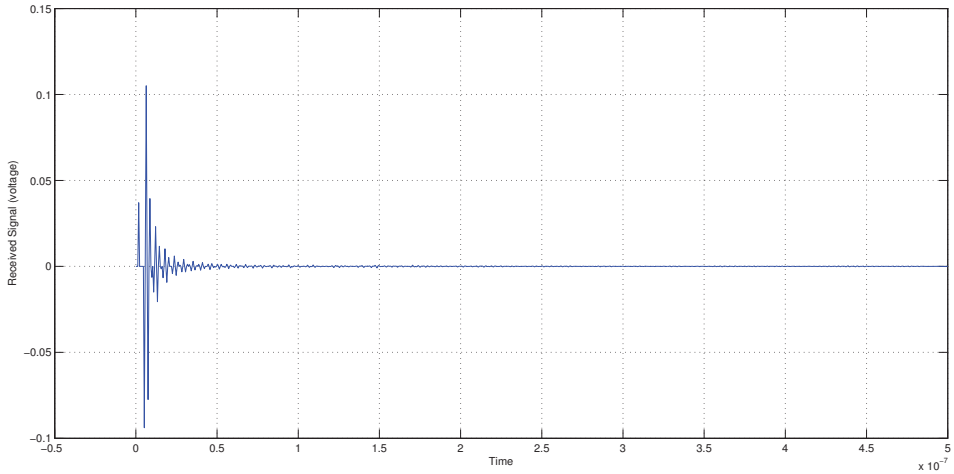

Figure 4.3: Free Space Received Signal and Associated Numerical Decay of the Algorithm

The time resolution of event-based TLM method is dependent upon the grid resolution chosen for the 3D mesh as follows:

$$dt = \frac{l}{\sqrt{3}c} \tag{4.11}$$

Where l is the grid resolution and c is the speed of light. For example, 1 meter grid resolution will have the transmit pulse width of approximately $2ns$. The minimum resolvable delay between multipath components using this method is given by dt. The selection of dt is dependent on the propagation frequency of interest. The grid resolution is chosen as at least half-wavelength of the frequency of interest to capture the reflections at the order of one wavelength within the environment. For example, grid resolution of $2.4GHz$ signal propagation is approximately $6cm$.

4.3 Simulator Setup and Experiments

The event-based TLM method simulator takes as input the 3-D CAD file of the building and draws a mesh based on the user-specified mesh-size. Typically the mesh

size is chosen to be $0.5 - 0.25$ times the wavelength of interest. This allows accurate computation of reflections from different materials of interest with in the environment. Figure 4.4 shows the snapshot of the 3-D model used for the simulations. The material properties (impedance (ohms) and attenuation(Nepers/m)) of various components in the 3-D model are given as input to the simulator using a text file. The simulator uses these values to compute the reflection and transmission coefficients at each junction direction. The simulator records voltages v received at a particular user-specified junction over the duration of the simulation. To demonstrate the impulse response

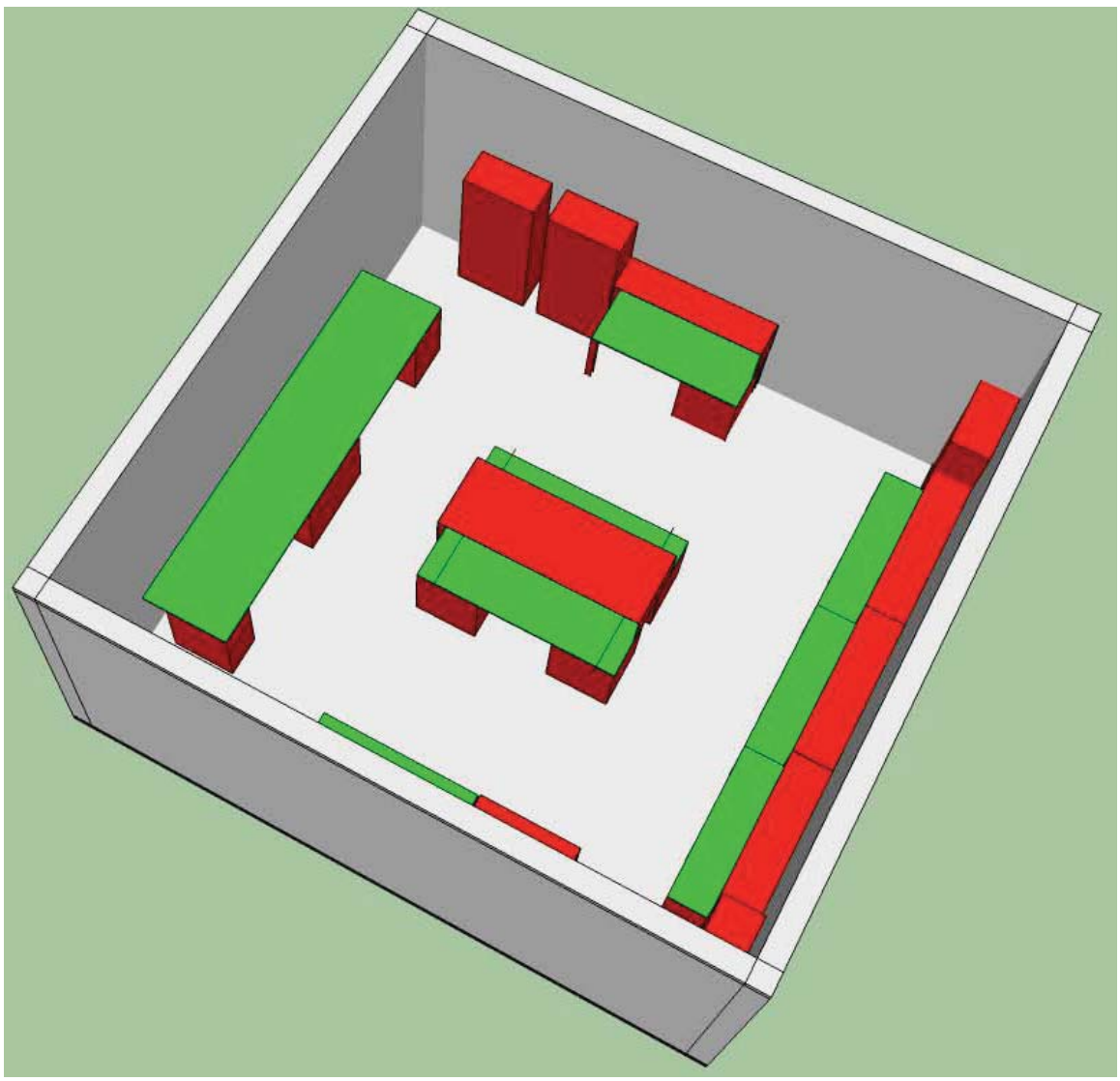

Figure 4.4: 3-D CAD File as Simulator Input

Figure 4.5: Free Space Box with Metal Wall

of the channel with multipath characteristics, a free space (air) box is created with one of the sides as a metal wall with zero impedance and attenuation, approximating a perfect reflecting surface for incident electromagnetic waves. Figure 4.5 shows the free space propagation environment with a metal wall. Figure 4.6 shows the slice of the simulation in the transmitter plane. Blue denotes the strongest signal and red denotes the weakest signal. The receiver lies in the center of the box. Figure 4.7 shows the received signal over the duration of the simulation. The time step is given by equation 4.11. Notice the line-of-sight (LOS) is the first strongest signal arriving at the receiver and the subsequent receptions are reflections from the metal wall. From [19] this received signal approximate the impulse response of the channel. Figure 4.8 gives the PDP of the channel with noticeable peaks, initial reception and subsequent four resolvable copies, depicting the multipath effects captured by the simulator.

While the free space with metal wall box is shown as a calibration example of the simulator, the simulator can take as input complex geometry for propagation modeling. Figure 4.9 is the simulated output of the room shown in Figure 4.4

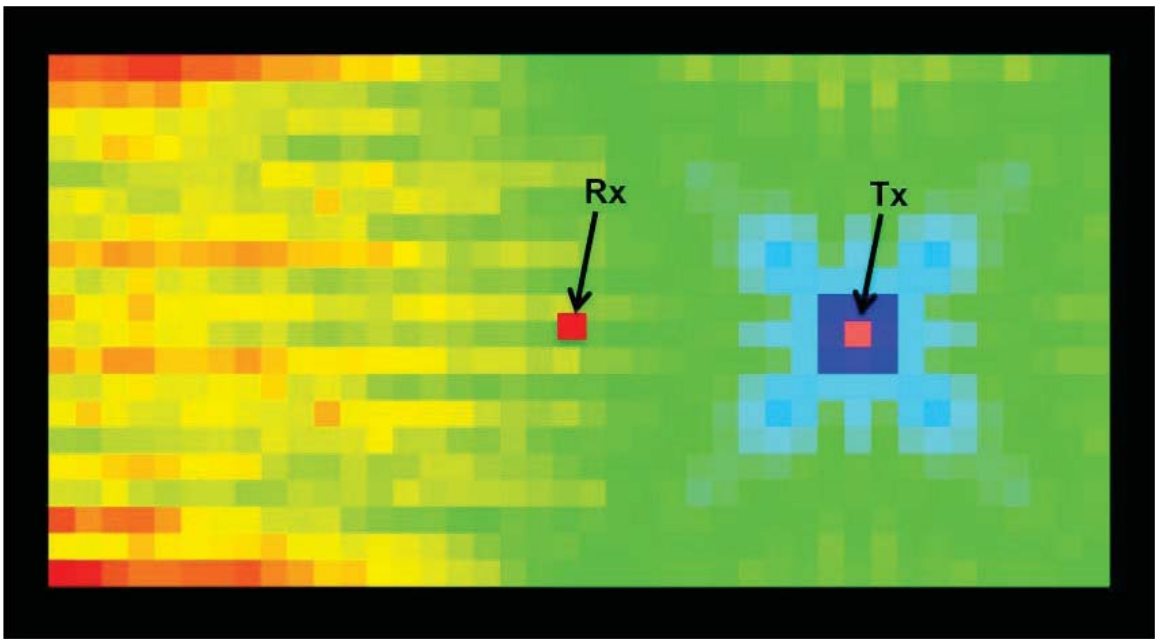

Figure 4.6: Free Space Box with Metal Wall Output of Simulator

consisting of cement, metal, and wood. The room is $8m$ x $8m$ x $4.5m$ in dimension and the simulation is done using a $5cm$ mesh-size. The time-domain received signal is recorded on the top left corner of the room in the same plane as transmitter.

Figure 4.10 shows the impulse response of the room and Figure 4.11 is the PDP of the room. The PDP reveals at least six significant paths. This demonstrates the ability to synthetically simulate site-specific channel impulse response and subsequently extract multipath characteristics of the environment. The mesh size is proportional to the resolvable multipath signals providing the flexibility to derive detailed channel characteristics with corresponding increase in computation time.

4.4 Conclusions and Future Work

Wide usage of wireless networks are beginning to require site-specific propagation models to assist in wireless network deployments. Event-based TLM method for wave propagation is demonstrated to extract multipath characteristics of the channel and serves a fast, accurate, site-specific in cluttered environments. The demonstrated

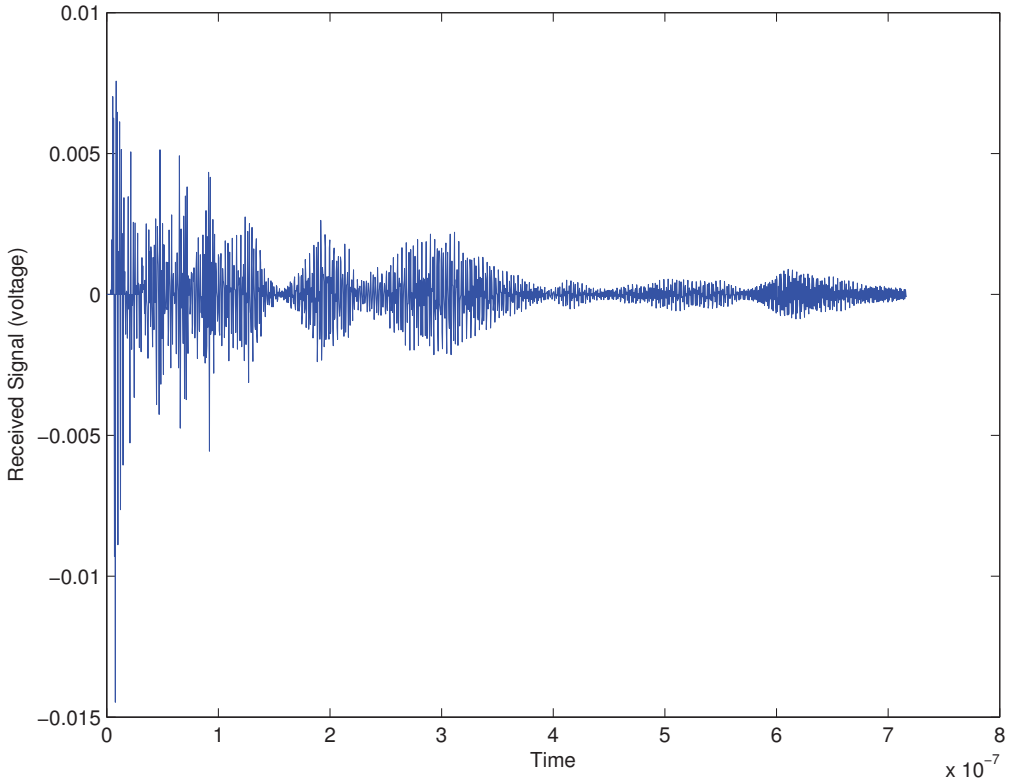

Figure 4.7: Impulse Response of Free space Box with Metal Wall

model is based on established transmission line matrix method that approximated Huygens' principle but with optimizations to restrict computations to the active wavefronts. The method is useful to approximate the influential multipath effects of the channel. Multipath effects can be destructive or constructive depending on the vector cancellations in the channel. If the symbol rate is less than the delay spread estimated for the channel, the communication can suffer from inter-symbol interference. In future work, the output of the simulator is validated using experimental data from pulse propagation measurement setup. Data for this validation is collected as shown in Figure 4.12 and 4.13. The output of the simulator can be used towards better communication parameter optimization including symbol rate, data rate, and frequency selection. The simulator currently uses a cubic 3D structure, this work can be extended to use spherical 3D structure

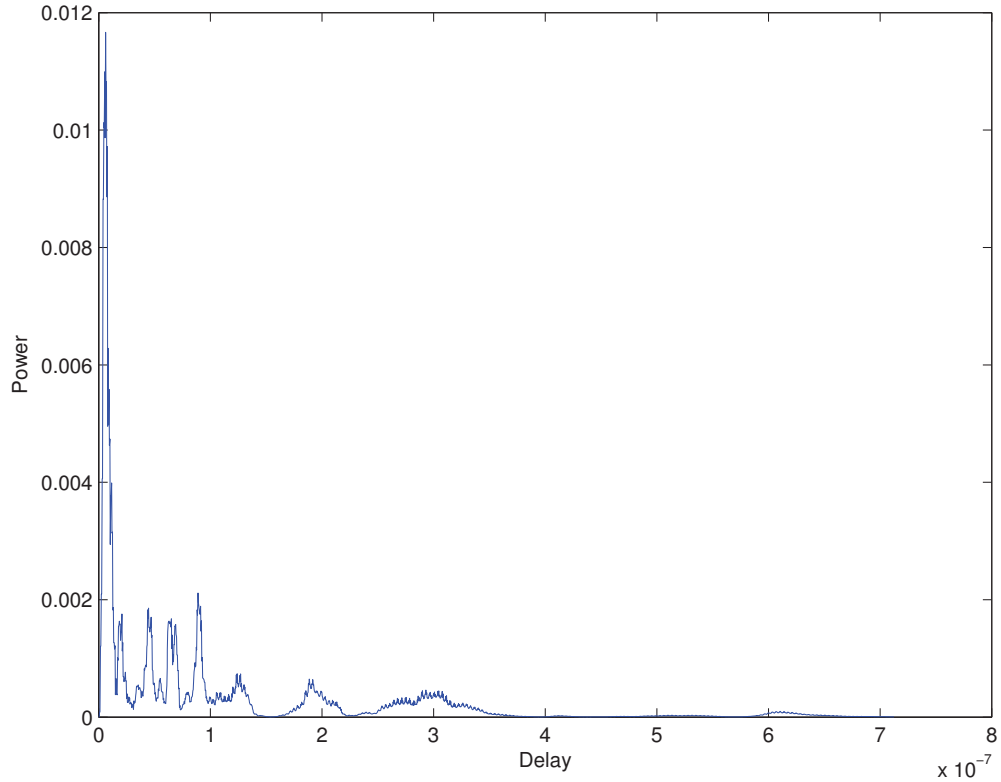

Figure 4.8: PDP of Free space Box with Metal Wall

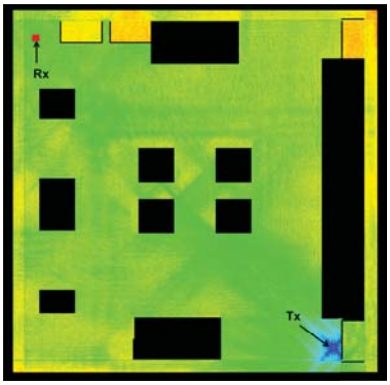

Figure 4.9: Propagation in Room

to explore the directionality (polarization) of propagation mechanism. This can assist in optimization of antennas for a given environment with specific materials. Further more, using the simulated pulse-propagation technique demonstrated here

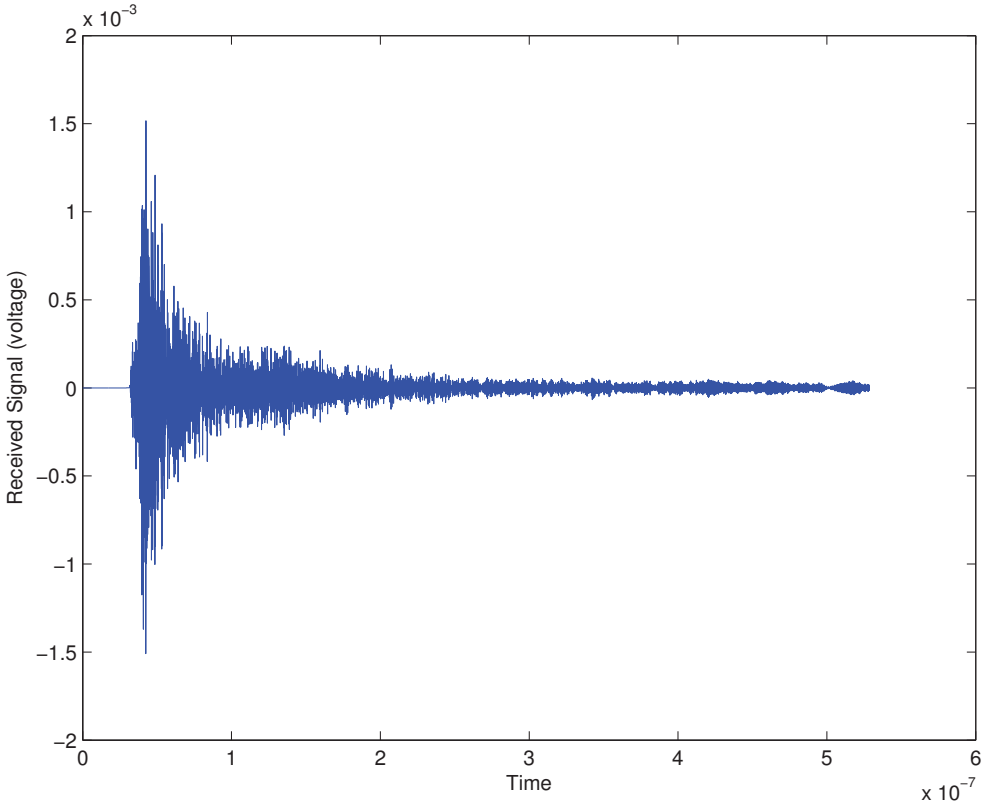

Figure 4.10: Impulse Response of Room

along with a packet-level network simulator, can assist in understanding the end-to-end performance of communication systems, particularly multiple-input multiple output (MIMO) systems. Capacity planning for micro- and femto-cell antennas for next generation urban cellular basestations can also be performed using this tool.

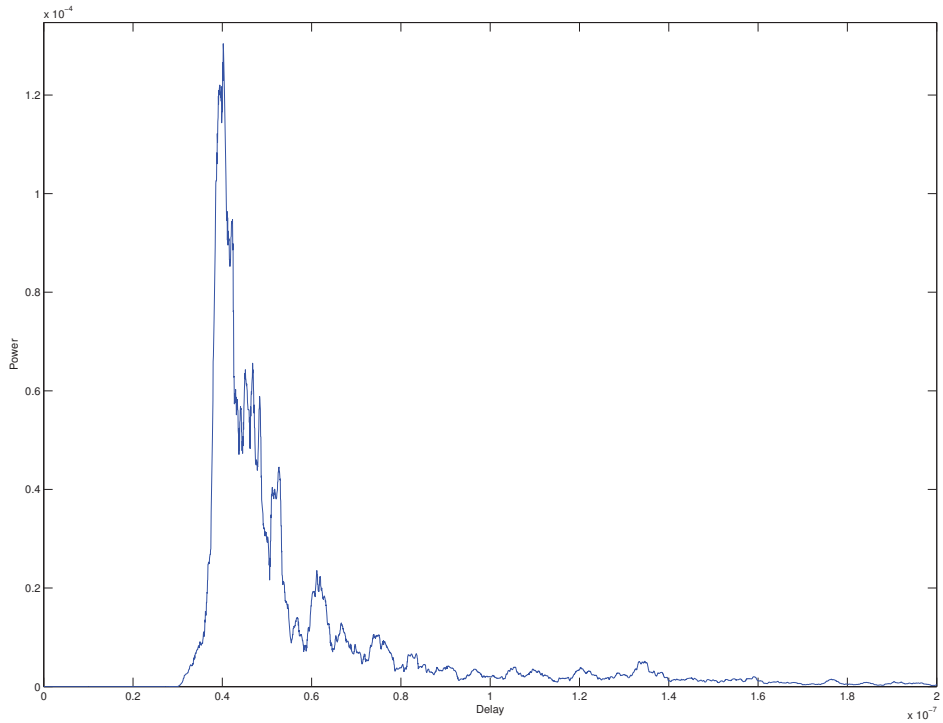

Figure 4.11: PDP of Room

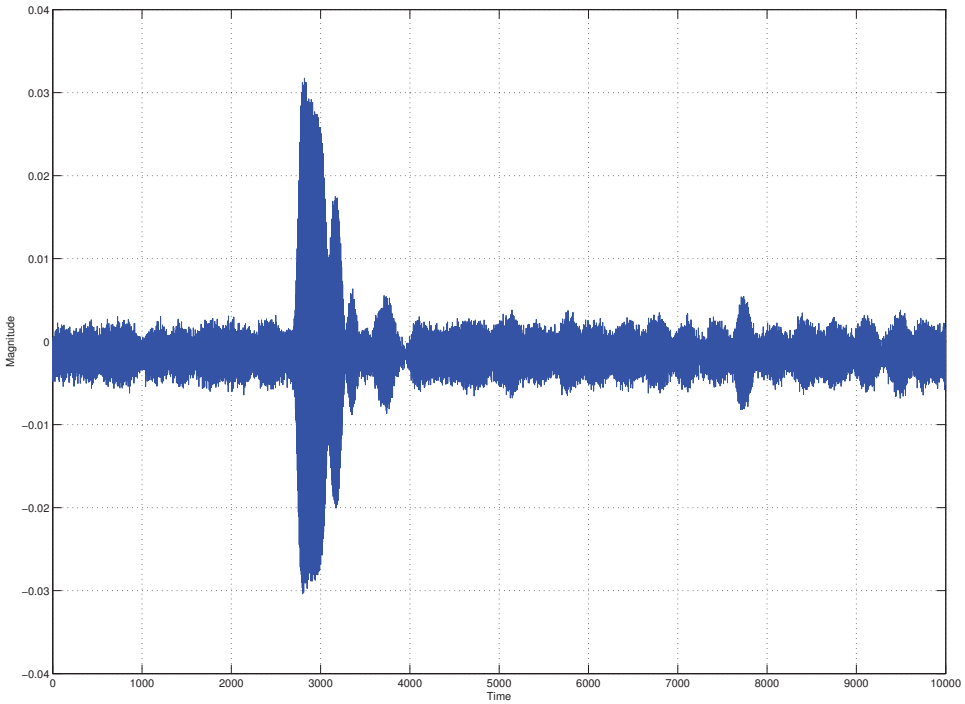

Figure 4.12: Received Signal of a Transmitted Pulse at Location 1

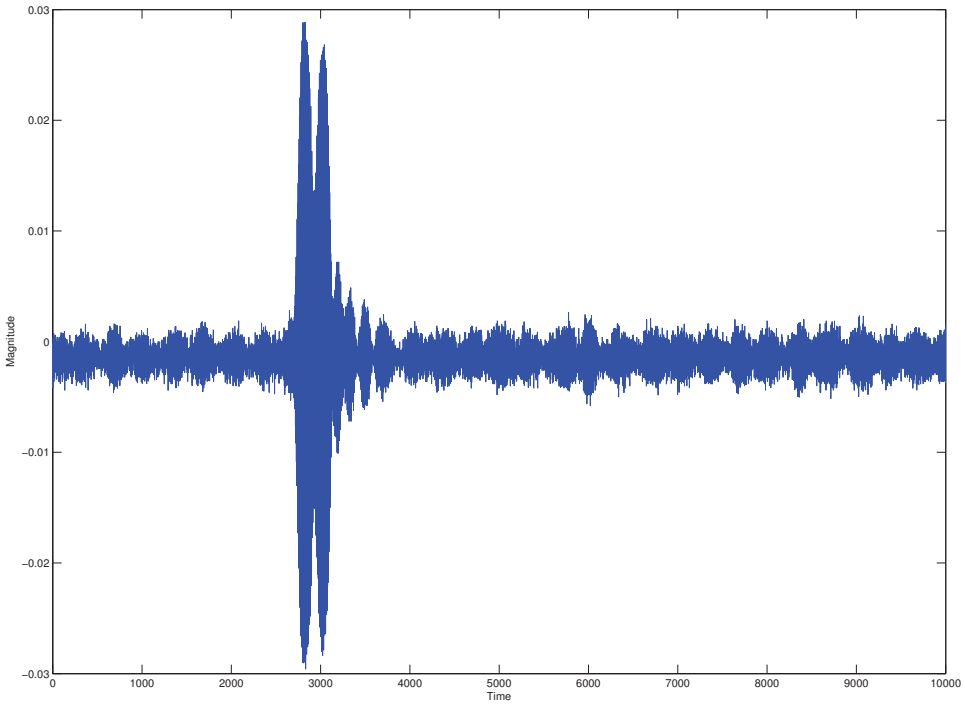

Figure 4.13: Received Signal of a Transmitted Pulse at Location 2

Chapter 5

Application of Channel Models

Accurate modeling of the propagation of radio waves is a critical shortcoming in existing, packet-level network simulation tools. Widely used simulators employ empirical models, such as the log-distance, two ray ground, and Raleigh and Rician fading models [43], to represent the radio channel. These models are designed for the general study of how network protocols behave in a typical propagation environment, but cannot predict performance within any specific environment.

New communication networks that are currently being, or planned to be, deployed will reside in cluttered environments for which empirical propagation models are not sufficient to determine if the network will deliver adequate performance. These future networking technologies include 3GPP Long Term Evolution (LTE), fourth generation (4G), industrial wireless networks (ISA 100, Wireless HART etc.), cellular infrastructure that uses medium- to small-sized base stations (often called femto-, micro-, pico-, and metro-cells; these support users in densely crowded, urban areas [35]). A characteristic of these new communication networks is that they reside in complex, sometimes highly metallic, environments and often operate without a line-of-sight between the transmitter and receiver.

Consequently, there is a growing interest in the modeling of radio propagation in complex environments [26][29][24]. The accurate modeling of radio channels is also

of considerable interest for Military Operations in Urban Terrain (MOUT), which, as rural populations migrate into large cities, are an increasingly important theatre for operations. While empirical models of propagation can represent behaviors that are typical of large-scale or small-scale, point-to-point radio channels, site-specific models are needed for the predicting performance of applications that require a deterministic quality of service (QoS) within a specific propagation environment.

Site specific predictions can be made with finite difference time domain (FDTD) models and ray tracing models, but these require significant computation and are therefore impractical to integrate with packet-level simulations of a communication network. In this chapter, we discuss the integration of the computationally efficient RCSIM propagation model, which is derived from the event-driven transmission line matrix method [38], with the ns-3 network simulator and how these collectively can be used to perform end-to-end-simulations of wireless networks. The RCSIM propagation model is described in Section 5.1 and its integration into ns-3 along with a case study of end-to-end simulation.

5.1 End-to-End Network Simulation

The event driven transmission line matrix (ETLM) method is based on a simple model of radio wave propagation through a homogeneous, three dimensional space. This simple model is given by the linear wave equation

$$\frac{\partial^2}{\partial t^2}U(t,x,y,z) = c^2\left(\frac{\partial^2}{\partial x^2} + \frac{\partial^2}{\partial y^2} + \frac{\partial^2}{\partial z^2}\right)U(t,x,y,z) \tag{5.1}$$

where t is time, c is the propagation speed, x, y, and z are Cartesian spatial coordinates, and $U(t,x,y,z)$ is the scalar electric field potential at the time-space coordinate (t,x,y,z). A discrete approximation of this partial differential can be constructed using finite-differences. This finite difference approximation can be viewed as a real valued cellular automaton (see, e.g., [52]). This cellular automaton

can, in turn, be optimized for computation by reinterpreting it as a discrete event system (see, e.g., [55]). The details of this transformation are given in [37, 38].

The fundamental computational element in this model is a junction structure that has a variable for the state v of the junction, six input variables $v_1^+, v_2^+, v_3^+, v_4^+, v_5^+, v_6^+$, and six output variables $v_1^-, v_2^-, v_3^-, v_4^-, v_5^-, v_6^-$. The state and output variables are computed by

$$v = \sum_{i=1}^{6} v_i^+ \tag{5.2}$$

$$v_i^- = \frac{v}{3} - v_i^+ \tag{5.3}$$

In an inhomogeneous space, different wave-carrying mediums are modeled as described above. The different media are joined using reflection and transmission junctions that model, respectively, reflection and transmission of the radio signal as it moves across the medium interface. A detailed description of the medium interface model can be found in [36] [38]. The resulting method is second order accurate within a homogeneous space and first order accurate at material interfaces.

The event-driven transmission line matrix method is implemented by the RCSIM simulator (see [44]), and can be invoked by NS3 to provide site-specific path loss and multipath characteristics. The RCSIM simulator uses a voxel-based model of the propagation environment to calculate a three dimensional map of the radio coverage provided by a transmitter located in a particular voxel. NS3 uses this capability in the following way to calculate the path-loss of a radio channel connecting a transmitter at location A with a receiver at location B.

1. At the start of a simulation, NS3 creates (or, optionally, reuses) a directory to cache the signal maps generated by RCSIM.

2. When a path-loss calculation is requested for a transmitter at position A and receiver at position B, NS3 first looks into a cache directory for a coverage map

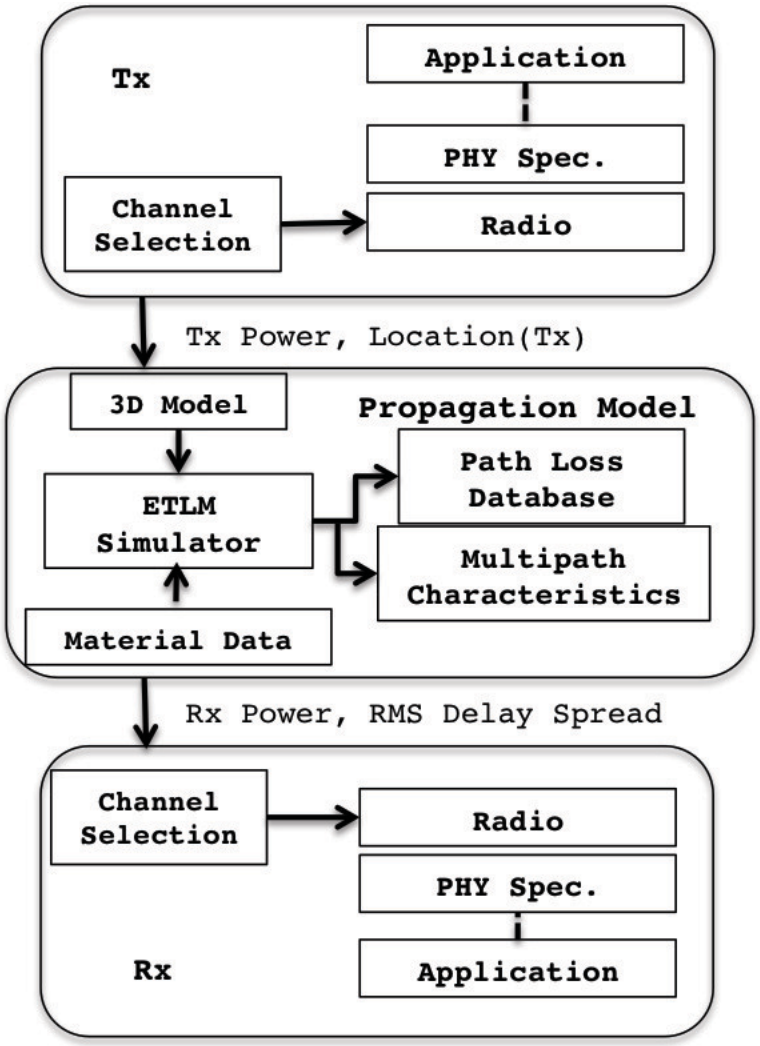

Figure 5.1: End-to-End Simulation Architecture

for a transmitter located at A. If this coverage map is found, then NS3 extracts the path-loss for location B and returns that value to the simulation.

3. If a coverage map is not found for the transmitter located at A, then NS3 invokes the RCSIM simulator to calculate this coverage map. The coverage map is then stored in the cache and the path-loss for the receiver at location B is extracted from the coverage map and returned to the simulation.

This propagation model for NS3 is implemented using the standard interface for radio propagation models in NS3, and so can be used interchangeable with the

empirical models provided in the NS3 package. Figure 5.1 shows the integrated simulation architecture. We take advantage of this to compare the path-loss predicted by site-specific and empirical models for the 3D model shown in Fig. 5.2. LTE

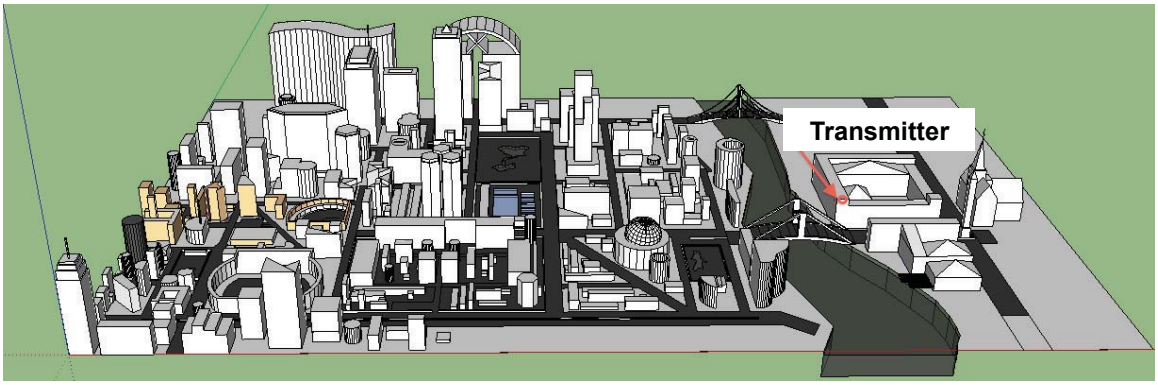

Figure 5.2: City Block Used for Demonstration

is a wireless networking system standardized by 3GPP to succeed the Universal Mobile Telecommunication System (UMTS) [1]. NS3 includes a module for simulating LTE [4] with empirical models of the path-loss of the radio channel. The downlink transmission of the LTE uses orthogonal frequency division multiplexing (OFDM) by converting single wide-band frequency selective channel to a multiple flat fading subchannels to improve downlink system performance. The LTE module described in [4] uses Jake's multipath fading model [43] along with empirical shadowing and penetration loss models to compute the received signal strength of a given subchannel.

Figure 5.3 compares simulations of the path-loss at a mobile, LTE receiver using the empirical model and RCSIM model for the path-loss component of the LTE propagation model. Figure 5.2 shows the propagation environment and transmitter. The site-specific simulations, which in this case combines empirical models for small-scale propagation phenomena with a site-specific model for large-scale propagation phenomena, captures critical effects, such as shadowing by the buildings (illustrated in Fig. 5.2), that are absent from the purely empirical model. The simulations based on RCSIM are therefore expected to provide more accurate predictions of system performance. Similarly, the WiFi channel models described in [3] can be enhanced in

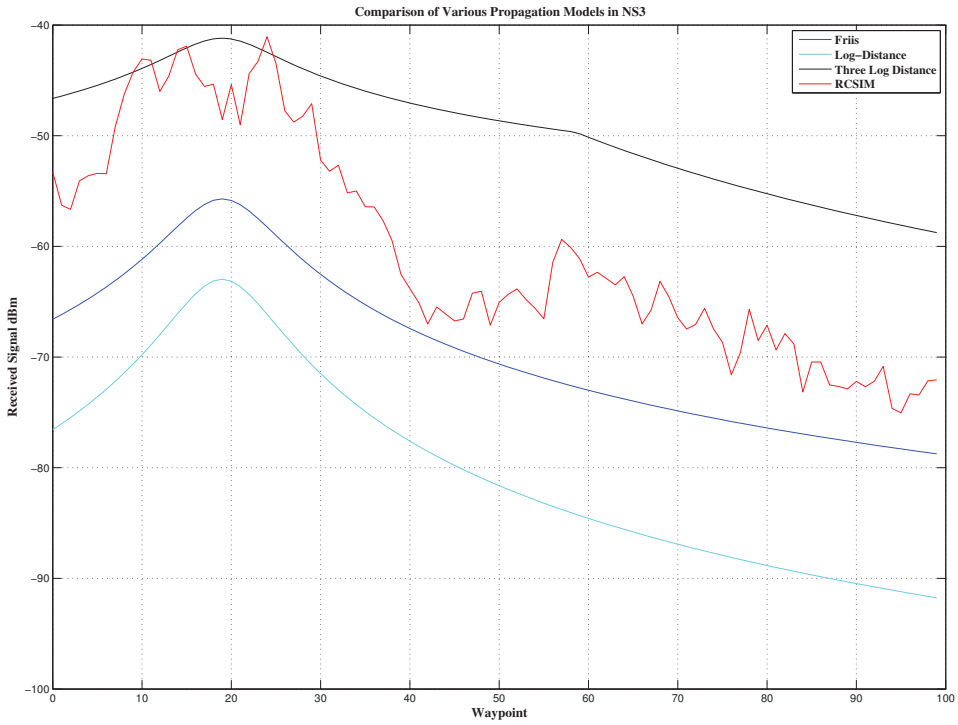

Figure 5.3: Comparison of Empirical and Site-specific Propagation Models

this way to provide site-specific predictions of application-level performance. Table 5.1 shows the comparison of various network performance indicators between two propagation models in an LTE uplink scenario. *TxBytes* and *RxBytes* denotes the number of radio link control (RLC) bytes transmitted and received. *PduSize* denotes the average size of the RLC protocol data unit (PDU). *min* and *max* denotes the minimum and maximum RLC PDU size. *MCS* denotes the modulation coding scheme selected by the device based on the channel quality indicator (CQI). *SE* denotes the spectral efficiency of the radio channel. The table shows that the end-to-end simulation provides differences in performance estimates based on the propagation model chosen.

Model	TxBytes	RxBytes	PduSize	min	max	MCS	SE
RCSIM	200210.38	199706	804.33	716.75	807	14	1.6953125
Freespace	419690.38	418632.88	1686.07	1491.13	1692	24	4.212890625

Table 5.1: Uplink Parameters With Different Propagation Models

5.2 Optimal Weights for Array Antenna

With the rapid growth in the networked environments for different industrial, scientific and defense applications, there is a vital need to assure the user or application a certain level of Quality of Service (QoS) in performing a particular transaction. For example, if an industrial site incorporates a distributed control of certain processing equipment or networked control of robots in the manufacturing plant, the QoS of the network carrying the control packets defines the functionality or performance of the industrial process. For a long time the QoS has been perceived as a quoted parameter of a particular network but not as a real-time measurable or quantifiable parameter. The bandwidth and throughput metrics of the entire network are dependent on the robust connectivity during topology formation. Deploying highly dense radios across a geographical area and the robust network formation of these radios continues to be a challenge. The key to the mesh formation is being aware of the network neighborhood, nature of the traffic in the network and information about the RF environment.

The different smart antennae technologies available [7] to accomplish robust network formulation are:

- Diversity: multiple antennas to spatially cover different areas.
- Switched Beamforming: A narrow band to service a predetermined area that is discretely selectable
- Adaptive Beam Forming: This is similar to switched beamforming but the selection of the beams is done in real-time using a feedback mechanism.

- Multi-input Multi-output (MIMO): Transmitting with multiple antennas and recollect the signals with multiple antennas achieving an improved spatial diversity and controllability.

The challenge as discussed in [47], [49], [5], [20], [13], it is evident that the capacity and the QoS of service of the WSN can be improved upon using a combination of adaptive, beamforming, reconfigurable antenna. [54], [56] demonstrate the measured and simulated results for MEMS-switched reconfigurable antennas. [20], [27] discuss the beamforming, reconfiguring and control schemes for antenna arrays.

Adaptive antenna is typically an array antenna whose pattern and frequency response can be controlled [18]. Typical interference patterns among multiple elements of modern wireless communication antennas is correlated and adaptive weights are needed to maximize signal to noise ratio [2]. Consider an Applebaum array, also known as Howells-Applebaum array, which focuses on maximizing the desired-to-undesired (interference and noise) signal ratio at the output of the array [18]. Figure 5.4 shows an N-element adaptive antenna array with arriving signals at each element $x_i(t)$ and weight of each element as w_i. The output of the array is shown as $y(t)$. The antenna input X, weights W, and output $y(t)$ are given by:

$$X = [x_1(t), x_2(t), ..., x_N(t)]^T \tag{5.4}$$

$$W = [w_1, w_2, ..., w_N]^T \tag{5.5}$$

$$y(t) = W^T X \tag{5.6}$$

In [18][2] it is shown that the optimum weights are determined by

$$MW = \mu S* \tag{5.7}$$

$$W = \mu M^{-1} S*, \tag{5.8}$$

Where M is the covariance of noise outputs from each element, μ is a scalar constant, and $S*$ represents the inter-element phase shifts and element patterns in

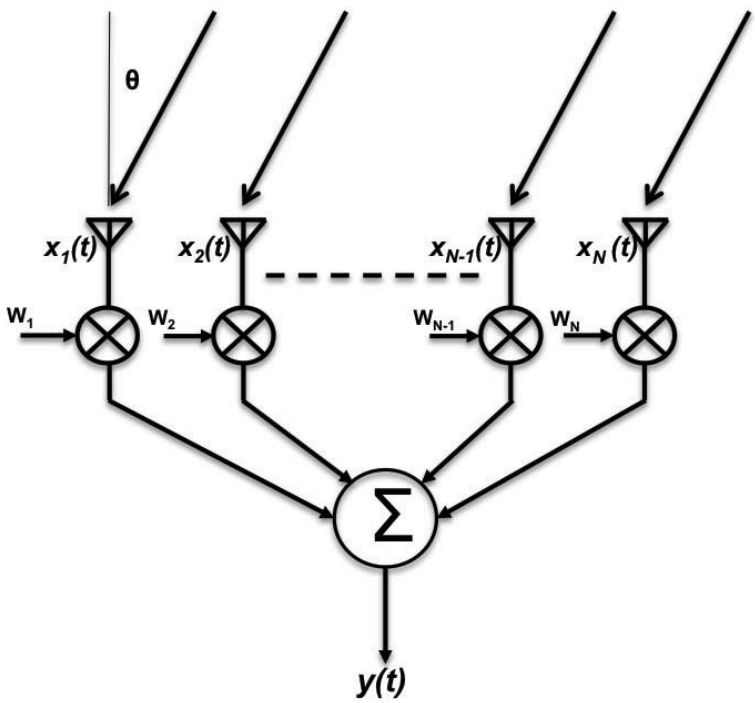

Figure 5.4: N-element Adaptive Antenna Array

the desired direction $\theta$from the mechanical boresight given by

$$M = [\mu_{kl}] \tag{5.9}$$

$$\mu_{kl} = E(n_k * n_l) \tag{5.10}$$

$$S = [s_1, s_2, ..., s_N] \tag{5.11}$$

$$s_k = exp\left(j\frac{2\pi kd}{\lambda}sin\theta\right) \tag{5.12}$$

Where n_k and n_l denote the noise in kth and lth channel and d is the element spacing and λ is the wavelength. The time-varying nature of the wireless channels is captured using stochastic differential equation (in continuous time) or a stochastic difference equation (in discrete time)[11] described in Chapter 2.

$$\begin{aligned} x_{t+1} &= A_t x_t + B_t w_t \\ y_t &= C_t x_t + D_t v_t \end{aligned} \tag{5.13}$$

where $x_t \in \Re^n$ is the state vector, $y_t \in \Re^d$ is a measurement vector sampled at the output of the channel, $w_t \in \Re^m$ is a state noise, and $v_t \in \Re^d$ is measurement noise. $\{A_t, B_t, C_t, D_t\}$ and states $\{x_t\}_t$ are the unknown parameters of the channel and shall be estimated using measurement data $\{y_t\}_t$. The time varying property of the parameters adapts dynamically to the variety of outputs. The Gaussian noise terms w_t and v_t can also capture the uncertainties introduced at each time step. Channel parameters $\theta = \{A_t, B_t, C_t, D_t\}$ can be estimated recursively using Expectation-Maximization(EM) algorithm. D_t represents the covariance of the noise at each time step and can be used for optimal weight computation. The ability to track the noise and interference is dependent upon the process chosen to represent the noise v_t. At each time step t the noise covariance can be computed and used for weights in time $t + 1$. This formulation enables application of real-time dynamic channel modeling to track undesired signals and improve signal to noise ratio of the adaptive antenna. Further research is required for improving the noise models to include discontinuous process, for e.g., using Levy process.

5.3 Conclusion

In this chapter a site-specific radio wave propagation model based on event-based TLM is integrated into a discrete-event based packet-level network simulator. This enables rigorous end-to-end performance measurements of wireless networks including LTE, industrial wireless network, and public WiFi networks. The event-based TLM ensures realistic computation time for these simulation (in the order of several minutes). Typical industrial environments have 3D computer aided design (CAD) models of the facility and 3D models of the urban areas are available in open source libraries like Google Sketchup. These models along with digital elevation maps can increase the accuracy of the application-level network performance simulations. An online stochastic estimation technique is formulated for recursive weight estimation of the multi-element array antenna.

Chapter 6

Conclusion

This study discussed the use of site-specific and dynamic channel models for improving the deployment and commissioning of wireless communication systems. We first measured the two potential forms of interference sources (1) wireless networks operating in the same frequency band whose operations are not coordinated, (2) industrial equipment producing wide-band interference in the same frequency band as the communication system.

Second, a wave propagation simulation is described that offers a fast, reasonably accurate, physically based, site specific method for calculating path-loss in cluttered environments. The simulation technique is derived from the well established transmission line matrix method. Two validation studies show that the method is suitable for generating grid based path-loss data that could be integrated with a mobile wireless network simulation. Applications of such an integrated simulator include, urban combat network planning and deployment, deployment of future combat systems, city-wide wireless network deployment, and industrial (RF harsh) wireless network deployment.

Third, a novel dynamic channel model based on expectation maximization and Kalman filter is demonstrated for recursive state estimation of the received signal. This model is demonstrated to provide accurate channel state estimation

and prediction of the received signal strength. Kalman filter and prediction error minimization techniques are demonstrated for one-step prediction. Two validation studies show the method is suitable for estimation and prediction. .

Fourth, event-based TLM method for wave propagation is demonstrated to extract multipath characteristics of the channel and serves a fast, accurate, site-specific method in cluttered environments. The demonstrated model is based on established transmission line matrix method that approximated Huygens' principle but with optimizations to restrict computations to the active wavefronts. The method is useful to approximate the influential multipath effects of highly cluttered environments. Measurement of multipath parameters is often times not possible. This simulation-based techniques provides accurate multipath parameter estimates that can be used for communication system design, configuration, and deployment.

Finally, applications of the site-specific and dynamic channel models is demonstrated using two applications. The site-specific radio wave propagation model based on event-based TLM is integrated into *NS3*, a discrete-event based packet-level network simulator. This enables rigorous end-to-end performance measurements of wireless networks including long term evolution (LTE), industrial wireless network, and public WiFi networks. The event-based TLM ensures realistic computation time for these simulation (in the order of several minutes). Typical industrial environments have 3D computer aided design (CAD) models of the facility and 3D models of the urban areas are available in open source libraries like Google Sketchup. These models along with digital elevation maps can increase the accuracy of the application-level network performance simulations. The dynamic channel models are used to derive the optimal weights of multi-input multi-output array antennas to counteract the noise and interference in the environment.

In future work, the dynamic channel models can be used for real-time applications like power control, adaptive antennas, and control over wireless networks. The model described in this research assumes Gaussian noise. However, perturbations induced by buildings are abrupt and can cause received signal measurements that are not

captured by assuming Gaussian measurement noise. These abrupt perturbations may be captured using Levy process. Alternatively the perturbations can be modeled using dual Gaussian processes to model the signal variations and abrupt changes respectively. The dynamic channel models, in its state-space representation, provides accurate estimation of the channel state and the time-varying properties of interference and noise. This model can be used to describe multi-input multi-output communication systems and can be used for optimizing the performance of adaptive antenna arrays, particularly in noisy environments.

Also, in future the output of the TLM-based simulator can be used towards better communication parameter optimization including symbol rate, data rate, and frequency selection. The simulator currently uses a cubic 3D structure, this work can be extended to use spherical 3D structure to explore the directionality (polarization) of propagation mechanism. This can assist in optimization of antennas for a given environment with specific materials. Further more, using the simulated pulse-propagation technique demonstrated along with a packet-level network simulator, can assist in understanding the end-to-end performance of communication systems, particularly multiple-input multiple output (MIMO) systems. Capacity planning for micro- and femto-cell antennas for next generation urban cellular basestations can also be performed using this tool.

Bibliography

[1] 3GPP. Technical specification group radio access network; (e-utra) and (e-utran). Technical report, 2008. 73

[2] Sidney P. Applebaum. Adaptive arrays. *IEEE Transactions on Antennas and Propagation*, AP-24(5):585–598, September 1976. 76

[3] Nicola Baldo and Marco Miozzo. Spectrum-aware channel and phy layer modeling for ns3. In *The network simulation tools workshop*, Pisa, Italy, October 2009. 73

[4] Nicola Baldo, Marco Miozzo, Manuel Requena-Esteso, and Jaume Nin-Guerrero. An open source product-oriented lte network simulator based on ns-3. In *Proceedings of the 14th ACM international conference on Modeling, analysis and simulation of wireless and mobile systems*, pages 293–298, Miami, Florida, USA, 2011. 73

[5] Lichun Bao and J.J. Garcia-Luna-Aceves. Transmission scheduling in ad hoc networks with directional antennas. In *Proceedings of the 8th annual international conference on Mobile computing and networking*, MobiCom '02, pages 48–58, New York, NY, USA, 2002. ACM. 76

[6] G. Bishop and G. Welch. An introduction to the kalman filters. University of North Carolina, 2001. 28

[7] Deepak Boppana and Asif Batada. How to create beam-forming smart antennas using fpgas, 2005. 75

[8] David Cavin, Yoav Sasson, and Andre Schiper. On the accuracy of MANET simulators. In *POMC '02: Proceedings of the second ACM international workshop on Principles of mobile computing*, pages 38–43, New York, NY, USA, 2002. ACM Press. 15

[9] C.D.Charalambous, R.J.C Bultitude, X. Li, and J. Zhan. Modeling wireless fading channels via stochastic differential equations: Identification and estimation based on noisy measurements. *IEEE Transactions on Wireless Communications*, 7(2):434–439, 2008. 22

[10] C.D.Charalambous and A. Logothetis. Maximum-likelihood parameter estimation from incomplete data via the sensitivity equations: The continuous time case. *IEEE Transactions on Automatic Control*, 45(5), 2000. 24, 25

[11] C.D.Charalambous, A. Logothetis, and R.J. Elliott. Bank filters for ml parameter estimation via the expectation-maximization algorithm: the continuois case. *IEEE Transactions on Automatic Control*, 1998. 23, 77

[12] Malgorzata Celuch-Marcysiak and Wojciech K. Gwarek. Generalized tlm algorithms with controlled stability margin and their equivalence with finite-difference formulations for modified grids. *IEEE Transactions on Microwave Theory and Techniques*, 43(9):2081–2089, 1995. 22, 57

[13] B.A. Cetiner, H. Jafarkhani, Jiang-Yuan Qian, Hui Jae Yoo, A. Grau, and F. De Flaviis. Multifunctional reconfigurable mems integrated antennas for adaptive mimo systems. *Communications Magazine, IEEE*, 42(12):62 – 70, dec. 2004. 76

[14] J.S. Chen and S.B. Hall. Efficient indoor and outdoor EM wave propagation in a compact terrain database (CTDB) representation of the urban canyon

environment. In *Proceedings of the IEEE 56th Vehicular Technology Conference (VTC 2002-Fall)*, volume 2, pages 802–806, 2002. 16, 17

[15] Katherine Chen and Carlos Guestrin. http://www.select.cs.cmu.edu/data/index.html. 45

[16] Zhongqiang Chen, Alex Delis, and Henry L. Bertoni. Radio-wave propagation prediction using ray-tracing techniques on a network of workstations (now). *Journal of Parallel and Distributed Computing*, 64(10):1127–1156, 2004. 17, 18

[17] Thomas Colegrove. AMSAA MOUT RF Propagation Model, January 2005. 16

[18] R.T. Compton. *Adaptive Antennas: Concepts and Performance*. Prentice Hall, 1988. 76

[19] D.C Cox. Delay doppler characteristics of multipath delay spread and average excess delay for 910 mhz urban mobile radio paths. *IEEE Transactions on Antennas and Propagation*, AP-20(5):625–635, September 1972. 53, 61

[20] Tassos Dimitriou and Antonis Kalis. Efficient delivery of information in sensor networks using smart antennas. In *In 1st International Workshop on Algorithmic Aspects of Wireless Sensor Networks (ALGOSENSORS 2004*, pages 109–122. Springer-Verlag, 2004. 76

[21] R.J. Elliott and V. Krishnamurthy. New finite-dimensional filters for parameter estimation of discrete-time linear guassian models. *IEEE Transactions on Automatic Control*, 44(5):938–951, 1999. 24, 26

[22] Ingo Gruber, Oliver Knauf, and Hui Li. Performance of ad hoc routing protocols in urban environments. In *Proceedings of European Wireless 2004 (EW'2004)*, Barcelona, Spain, February 2004. 15

[23] Ingo Gruber and Hui Li. Behavior of ad hoc routing protocols in metropolitan environments. In *Proceedings of the 60th IEEE Vehicular Technology Conference (VTC2004-Fall)*, volume 5, pages 3175–3180, 2004. 15

[24] Keith T. Herring, Jack W. Holloway, David H. Staelin, and Daniel W. Bliss. Path-loss characteristics of urban wireless channels. *IEEE Transactions on Antennas and Propagation*, 58(1):171–177, January 2010. 16, 69

[25] Wolfgang J.R. Hoefer. The transmission-line matrix method - theory and applications. *IEEE Transactions on Microwave Theory and Techniques*, MTT-33(10):882–893, October 1985. 58

[26] Ivan Howitt, Wayne Manges, Teja Kuruganti, Glenn Allgood, Jose Gutierrez, and James Conrad. Wireless industrial sensor netwotks: Framework for qos assessment and qos management. *ISA Transactions*, 45(3):347–359, July 2006. 5, 69

[27] Y. Irie, S. Hara, Y. Nakaya, T. Toda, and Y. Oishi. A beamforming method for a reactively steered adaptive array antenna with rf-mems device. In *Wireless Communication Technology, 2003. IEEE Topical Conference on*, pages 396 – 397, oct. 2003. 76

[28] G. Kallianpur. *Stochastic Filter Theory*. Springer-Verlag, 1980. 29

[29] Snorre Kjesbu and Torkil Brunsvik. Radiowave propagation in industrial environments. In *26th Annual Industrial Electronics Conference*, volume 4, pages 2425–2430. IEEE Industrial Electronics Society, 2000. 5, 69

[30] Teja Kuruganti, Wayne Manges, Stephen Smith, and Davis Shull. Short range wireless sensor networks for proactive health monitoring of aging nuclear power plants. In *Proceedings of ANS Annual Meeting 2009*, 2009. 6

[31] Yanyan li, Mohammed Olama, Seddik Djouadi, Aly Fathy, and Teja Kuruganti. Uwb indoor wireless channel modeling and estimation from received signal

measurements. In *Proceedings of the IEEE Radio and Wireless Symposium*, pages 195–198, 2009. 22

[32] G. Liang and H.L. Bertoni. A new approach to 3-D ray tracing for propagation prediction in cities. *IEEE Transactions on Antennas and Propagation*, 46(6):853–863, June 1998. 17

[33] L. Ljung. *System Identification: Theory for the User*. Prentice Hall PTR, Upper Saddle River, New Jersey, 1999. 44

[34] Pascal O. Luthi, Bastien Chopard, and Jean-Frédéric Wagen. Wave Propagation in Urban Microcells: a Massively Parallel Approach Using the TLM Method. In *PARA '95: Proceedings of the Second International Workshop on Applied Parallel Computing, Computations in Physics, Chemistry and Engineering Science*, pages 408–418, London, UK, 1996. Springer-Verlag. 16

[35] Rick Merritt. Small basestations will be big:http://www.eetimes.com/electronics-news/4373380/small-basestations-will-be-big. *EE Times*, 2012. 69

[36] James Nutaro. A discrete event method for wave simulation. *ACM Transactions on Modeling and Computer Simulation*, 16(2):174–195, 2006. 16, 21, 31, 55, 56, 71

[37] James Nutaro and Phani Teja Kuruganti. Fast, accurate rf propagation modeling and simulation tool for highly cluttered environments. In *Proceedings of IEEE MILCOM 2007*, 2007. 21, 55, 71

[38] James Nutaro, Phani Teja Kuruganti, Rajanikanth Jammalamadaka, Tomas Tinoco, and Vladamir Protopopescu. An event driven, simplified tlm method for predicting path-loss in cluttered environments. *IEEE Transactions on Antennas and Propagation*, 56(1):189–198, January 2008. 21, 55, 56, 70, 71

[39] President's Committee of Advisors on Science and Technology. Federal energy research and development for the challenges of the 21st century. *Energy Research and Development Panel*, 3-16, November 1997. 1

[40] M. Olama, K.K. Jaladhi, S.M. Djouadi, and C.D. Charalambous. Recursive estimation and identification of time-varying long-term fading channels. *Research Letters in Signal Processing*, 2007. 42

[41] Mohammed Olama, Seddik Djouadi, and Charalambos Charalambous. Stochastic power control for time-varying long-term fading wireless networks. *EURASIP Journal on Applied Signal Processing*, pages 1–13, 2006. 22

[42] Mohammed Olama, Seddik Djouadi, and Charalambos Charalambous. Stochastic differential equations for modeling, estimation and identification of mobile-to-mobile communication channels. *IEEE Transactions on Wireless Communications*, 8(4):1754–1763, April 2009. 22

[43] Theodore S. Rappaport. *Wireless communications: principles and practice*. Prentice Hall PTR, Upper Saddle River, New Jersey, 1996. 2, 3, 4, 5, 16, 53, 54, 69, 73

[44] RCSIM-Manual, 2012. 71

[45] Remcom. Remcom wireless insite. 33

[46] K.A. Remley, A. Weisshaar, and H.R. Anderson. A comparative study of ray tracing and FDTD for indoor propagation modeling. In *Proceedings of the 48th IEEE Vehicular Technology Conference (VTC 98)*, volume 2, pages 865–869, 1998. 16, 17

[47] A.K. Saha and D.B. Johnson. Routing improvement using directional antennas in mobile ad hoc networks. In *Global Telecommunications Conference, 2004. GLOBECOM '04. IEEE*, volume 5, pages 2902 – 2908 Vol.5, nov.-3 dec. 2004. 76

[48] N.R.S. Simons and E. Bridges. Equivalence of propagation characteristics for the transmission-line matrix and finite-difference time domain methods in two dimensions. *IEEE Transactions on Microwave Theory and Techniques*, 39(2):354–357, 1991. 22, 57

[49] A. Spyropoulos and C.S. Raghavendra. Capacity bounds for ad-hoc networks using directional antennas. In *Communications, 2003. ICC '03. IEEE International Conference on*, volume 1, pages 348 – 352 vol.1, may 2003. 76

[50] Allen Taflove and Susan Hagness. *Computational Electrodynamics: The Finite-Difference Time-Domain Method, 3rd edition*. Artech House, Boston, MA, 2005. 16

[51] Ying Wang, S. Safavi-Naeini, and S.K. Chaudhuri. A hybrid technique based on combining ray tracing and FDTD methods for site-specific modeling of indoor radio wave propagation. *IEEE Transactions on Antennas and Propagation*, 48(5):743–754, May 2000. 17, 18

[52] Stephen Wolfram. *A new kind of science*. Wolfram Media, Inc., 2002. 21, 55, 70

[53] Chang-Fa Yang, Boau-Cheng Wu, and Chuen-Jyi Ko. A ray-tracing method for modeling indoor wave propagation and penetration. *IEEE Transactions on Antennas and Propagation*, 46(6):907–919, June 1998. 17, 18

[54] Songnan Yang, H.K. Pan, A.E. Fathy, S. El-Ghazaly, and V.K. Nair. A novel reconfigurable maze antenna for multi-service wireless universal receivers. In *Radio and Wireless Symposium, 2006 IEEE*, pages 195 – 198, jan. 2006. 76

[55] Bernard P. Zeigler, Herbert Praehofer, and Tag Gon Kim. *Theory of Modeling and Simulation, 2nd Edition*. Academic Press, 2000. 21, 55, 71

[56] Chunna Zhang, Yongping Han, Songnan Yang, A.E. Fathy, S. El-Ghazaly, and V.K. Nair. Multi-standard wireless receiver utilizing reconfigurable antennas and

rf front ends. In *Radio and Wireless Symposium, 2006 IEEE*, pages 399 – 402, jan. 2006. 76

[57] Yuhao Zheng and David M. Nicol. Validation of radio channel models using an anechoic chamber. In *Principles of Advanced and Distributed Simulation (PADS), 2010 IEEE Workshop on*, 2010. 30

Vita

Teja Kuruganti received his Bachelor of Engineering in Electronics and Communications Engineering from the Osmania University in 2001. He went to graduate school at the University of Tennessee, Knoxville, receiving Master's Degree in Computer Engineering in 2003 with a Master's Thesis titled "Development of Mobile Agent Framework in Wireless Sensor Networks for Multi-Sensor Collaborative Processing" under the direction of Dr. Hairong Qi. He then began a career at Oak Ridge National Laboratory with Modeling and Simulation Group of the Computational Sciences and Engineering Division. His research interests include wireless sensor networks and propagation modeling in harsh environments, modeling control systems operating over communication networks, cybersecurity of process control systems and collaborative signal and information processing in sensor networks. He worked on developing robust, reliable wireless sensor technology for harsh environments. He has developed and deployed wireless sensors for improving energy efficiency of buildings, steam lines, industrial process monitoring, and nuclear applications. He won an R&D 100 award in 2012 for co-developing novel electromagnetic wave propagation simulation engine for rapid deployment of wireless networks particularly in harsh environment applications. He restarted his academic pursuits, taking courses part-time and pursuing PhD degree in Electrical Engineering under the supervision of Dr. Seddik Djouadi.